

HCN Survey of Normal Spiral, IR-luminous and Ultraluminous Galaxies

Yu Gao^{1,2,3} and Philip M. Solomon⁴

ABSTRACT

We report systematic HCN J=1-0 (and CO) observations of a sample of 53 infrared (IR) and/or CO-bright and/or luminous galaxies, including seven ultraluminous infrared galaxies, nearly 20 luminous infrared galaxies, and more than a dozen of the nearest normal spiral galaxies. This is the largest and most sensitive HCN survey of galaxies to date. All galaxies observed so far follow the tight correlation between the IR luminosity L_{IR} and the HCN luminosity L_{HCN} initially proposed by Solomon, Downes, & Radford, which is detailed in a companion paper. We also address here the issue of HCN excitation. There is no particularly strong correlation between L_{HCN} and the $12\mu\text{m}$ luminosity; in fact, of all the four *IRAS* bands, the $12\mu\text{m}$ luminosity has the weakest correlation with the HCN luminosity. There is also no evidence of stronger HCN emission or a higher ratio of HCN and CO luminosities $L_{\text{HCN}}/L_{\text{CO}}$ for galaxies with excess $12\mu\text{m}$ emission. This result implies that mid-IR radiative pumping, or populating, of the J=1 level of HCN by a mid-IR vibrational transition is not important compared with the collisional excitation by dense molecular hydrogen. Furthermore, large velocity gradient calculations justify the use of HCN J=1-0 emission as a tracer of high-density molecular gas ($\gtrsim 3 \times 10^4/\tau \text{ cm}^{-3}$) and give an estimate of the mass of dense molecular gas from HCN observations. Therefore, L_{HCN} may be used as a measure of the total mass of dense molecular gas, and the luminosity ratio $L_{\text{HCN}}/L_{\text{CO}}$ may indicate the fraction of molecular gas that is dense.

¹Purple Mountain Observatory, Chinese Academy of Sciences, 2 West Beijing Road, Nanjing 210008, P.R. China

²Department of Astronomy, University of Massachusetts, LGRT-B 619E, 710 North Pleasant Street, Amherst, MA 01003

³Infrared Processing and Analysis Center, California Institute of Technology, MS 100-22, Pasadena, CA 91125

⁴Department of Physics & Astronomy, SUNY at Stony Brook, Stony Brook, NY 11794

Subject headings: galaxies: infrared — galaxies: ISM — galaxies: starburst —
ISM: molecules — radio lines: galaxies — surveys

1. INTRODUCTION

Though CO traces most of the molecular gas mass in galaxies, it does not necessarily trace active star-forming regions where the gas density is more than 10 times higher than the average. These regions are better traced by high dipole moment molecules like HCN, CS and HCO⁺. Consequently, these molecules have often been used as probes of physical conditions in giant molecular cloud (GMC) cores — the regions of active star formation in the Milky Way. Yet there have been few systematic studies of dense gas in GMCs in the disk of the Milky Way. Lee, Snell, & Dickman (1990) have found that for Milky Way disk GMCs, the ratio of CO/CS intensity is 156, much larger than for Galactic center clouds and an order of magnitude larger than for the archetypal ULIG Arp 220 (Solomon, Radford, & Downes 1990). Some dense clumps in some nearby GMCs have also been surveyed in CS (Lada, Bally, & Stark 1991; Plume et al. 1997) and in HCN (Helfer & Blitz 1997b). Although there are some recent attempts in Galactic plane HCN, CS, and CO observations (Helfer & Blitz 1997b; McQuinn et al. 2002 and references therein), only the central region of the Galaxy has been extensively mapped with dense molecular gas tracers (e.g., CS, Bally et al. 1987, 1988; HCN, Jackson et al. 1996; Lee 1996). Systematic and unbiased large-scale observations of the dense molecular gas in Galactic disk GMCs need continued study since the large-scale (kpc) distribution of dense gas in the Milky Way disk (cf. McQuinn et al. 2002) is a basis for comparison with dense molecular gas observations in external galaxies (e.g., Paglione et al. 1998).

HCN and CS are probably the most frequently observed interstellar molecules after CO. Because of their higher dipole moments ($\mu_0 \sim 2.0 - 3.0$ D), they require about 2 orders of magnitude higher densities for collisional excitation than CO ($\mu_0 \sim 0.1$ D). HCN is one of the most abundant high dipole moment molecules and traces molecular gas at densities $n(\text{H}_2) \gtrsim 3 \times 10^4 / \tau \text{ cm}^{-3}$ (compared to densities at $\gtrsim 500 \text{ cm}^{-3}$ traced by CO). HCN J=1-0 emission has been so far detected toward the nuclei of ~ 10 nearby galaxies (Nguyen-Q-Rieu, Nakai, & Jackson 1989; Nguyen-Q-Rieu et al. 1992; Henkel et al. 1990), 10 relatively distant luminous and ultraluminous infrared galaxies (LIGs and ULIGs with IR luminosities⁵ $L_{\text{IR}} > 10^{11} L_{\odot}$ and $> 10^{12} L_{\odot}$, respectively) including three less luminous,

⁵The total IR luminosity (from 8 μm to 1000 μm) is calculated according to the prescription in Sanders & Mirabel (1996) using measurements from all 4 *IRAS* flux bands.

“normal” spiral galaxies (Solomon, Downes, & Radford 1992), 12 nearby starburst and/or normal galaxies (Helfer & Blitz 1993), 10 interacting galaxies and infrared galaxy mergers (Aalto et al. 1995), 13 Seyfert galaxies (Curran, Aalto, & Booth 2000), and a few nearby CO-bright galaxies (Israel 1992; Sorai et al. 2002; Kuno et al. 2002). There are significant overlaps in the galaxy samples among these various observations, and the total number of galaxies with HCN detections is still $\lesssim 30$, particularly the total HCN emission measured globally from the galaxies. A recent summary of HCN observations in centers of nearby galaxies can be found in Sorai et al. (2002) and Shibatsuka et al. (2003).

In a few of the nearest galaxies, interferometer HCN maps have also been obtained in the nuclear regions (Carlstrom et al. 1988; 1990; Radford et al. 1991; Downes et al. 1992; Brouillet & Schilke 1993; Jackson et al. 1993; Helfer & Blitz 1995, 1997a; Tacconi et al. 1994; Shen & Lo 1995; Paglione, Tosaki, & Jackson 1995b; Kohno et al. 1996; Kohno, Kawabe, & Vila-Vilaro 1999). CS emission, another dense molecular gas tracer, has been observed in the central regions of ~ 10 galaxies as well including interferometry imaging (Mauersberger & Henkel 1989; Mauersberger et al. 1989; Sage, Shore, & Solomon et al. 1990; Helfer & Blitz 1993; Xie, Young, & Schloerb 1994; Paglione et al. 1995a; Peng et al. 1996; Reynaud & Downes 1997; Wild & Eckart 2000). The presence of large amounts of dense molecular gas in the central ~ 1 kpc of galaxies has been well established (for an earlier review, see Mauersberger & Henkel 1993).

The main goal of this paper is to present a systematic HCN survey of a large sample of normal spiral galaxies and relatively distant LIGs and ULIGs. This includes an attempt to measure the total HCN emission in nearby large spiral galaxies by mapping the HCN distribution along the major axes (Gao 1996, 1997). We examine correlations between HCN emission and various *IRAS* bands and discuss the excitation mechanisms of HCN. We here argue that HCN is primarily excited by collision with molecular hydrogen at high density and thus can be used as a tracer of dense molecular gas. We concentrate here on presenting observations of HCN J=1-0 only since it is almost always the strongest line among these high dipole moment molecules, and thus the easiest and most often observed dense gas tracer in external galaxies (Gao 1996). We have not only doubled the total number of galaxies with HCN J=1-0 detections in the literature for the last decade, but we have also extensively mapped the inner disk HCN emission in a few nearby galaxies in order to estimate the total HCN emission. We will explore in detail the extent and radial distribution of dense molecular gas in nearby galaxies in a future paper and present the detailed HCN mapping observations there (Y. Gao & P.M. Solomon in preparation). In a companion paper (Gao & Solomon 2004, Paper II), we fully discuss the interpretation and implications of our HCN survey.

We describe the sample selection and characteristics of our HCN survey in the next section. In § 3, we discuss our various observations and the observational strategies conducted at different telescopes. The survey results are presented in § 4, where we show all the HCN J=1-0 and CO spectra, tabulate the observational data, and summarize the global quantities for all galaxies. We have confirmed the tight correlation between the IR and HCN emission, initially proposed by Solomon et al. (1992) based on the HCN observations of a sample of 10 representative galaxies, in a large and statistically significant sample of more than 60 galaxies when both samples are combined. We have also checked for any significant dependence of the HCN emission upon the excess mid-IR emission as indicated by an *IRAS* flux ratio of the 12 and 100 μm emission or the ratio of the 12 μm and total IR emission to address the possibly enhanced excitation of HCN J=1-0 emission by mid-IR radiative pumping through a vibrational transition. Moreover, the use of HCN as a tracer of high-density molecular gas is discussed using large velocity gradient (LVG) calculations. Finally, we summarize the main points of this HCN survey in § 5.

2. THE HCN SURVEY SAMPLE

Our goal is to survey a large sample of galaxies (> 50) with a wide range of IR luminosities where the total HCN J=1-0 emission from the whole inner disk or entire galaxy can be measured. Essentially, all galaxies with strong CO and IR emission were chosen for our HCN observations. Our HCN survey sample is mainly drawn from the CO observations of Solomon et al. (1997), Sanders, Scoville, & Soifer (1991), Tinney et al. (1990), Solomon & Sage (1988), and Young et al. (1989, 1995). Almost all galaxies with an antenna temperature measured by various telescopes to be greater than 100 mK (or 50 mK for LIGs) were included as candidate galaxies. These cutoffs were specifically used in order to select all truly CO-bright galaxies in the hope of detecting their HCN emission (which is typically 10–20 times weaker than CO) with a rms sensitivity at the level of ~ 1 mK. Most IR-bright galaxies with $f_{60\mu\text{m}} > 50\text{Jy}$, or $f_{100\mu\text{m}} > 100\text{Jy}$ are included as well in our sample (Rice et al. 1988; Strauss et al. 1992). We thus selected ~ 10 nearest CO and/or IR bright large galaxies with $cz \lesssim 1,000 \text{ km s}^{-1}$ and $D_{25} \gtrsim 10'$, and a few tens of relatively distant yet still nearby “normal” spiral galaxies and LIGs. Moreover, most northern ULIGs in the local universe ($cz < 20,000 \text{ km s}^{-1}$) were also added to enlarge our sample at this extremely high IR luminosity.

We detected HCN J=1-0 emission from 52 galaxies, and only one galaxy was not detected. Table 1 lists all 53 sources, along with some basic properties of the galaxies useful for our observations and data analysis. The nearest large galaxies that require

mapping to estimate the total HCN emission are highlighted in boldface in Table 1, and the detailed observational results of these galaxies will be discussed separately (Y. Gao & P.M. Solomon 2004, in preparation). Seven ULIGs are marked with a star symbol in Table 1. Our HCN survey sample also contains essentially a statistically complete sample for northern ($\delta \geq -35^\circ$) galaxies with $f_{100\mu\text{m}} \geq 100$ Jy, which includes about 30 of the brightest *IRAS* galaxies.

For the purpose of the detailed statistical analysis to be presented in Paper II, we included almost all HCN data available in the literature where the total HCN emission from galaxies can be estimated to augment our sample. There are about a dozen mostly IR-luminous galaxies with total HCN emission measured, almost entirely from Solomon et al. (1992), but M51 and NGC 4945 are from Nguyen-Q-Rieu et al. (1992) and Henkel et al. (1990), respectively. Even with these supplements and those intentionally added ULIGs, the survey sample is not severely biased toward the high IR luminosity end. As shown in Figure 1a, although most of our sample galaxies are IR bright or the brightest in the local universe, more than half have IR luminosities less than $10^{11}L_\odot$, and among them most have $L_{\text{IR}} < 3 \times 10^{10}L_\odot$. There seems to be a slight bias, however, toward high CO luminosity galaxies (Fig. 1b), i.e., more CO-luminous or molecular gas-rich galaxies have been selected. This bias mainly arises because most normal spiral galaxies selected are CO bright and quite rich in molecular gas, and essentially all LIGs and ULIGs have high CO luminosities. Nevertheless, the galaxy number distribution in HCN luminosity appears to be rather unbiased with comparable numbers of galaxies with both low and high HCN luminosities, and the entire HCN luminosity distribution covers a large range of almost 3 orders of magnitude (Fig. 1c).

3. OBSERVATIONS

We used the former NRAO⁶ 12m telescope at Kitt Peak and the IRAM 30m telescope at Pico Veleta near Granada, Spain, for most of our HCN observations. The FCRAO⁷ 14m telescope with the 15 element focal-plane array receiver, QUARRY (a configuration of three rows of five beams with a row spacing of $100''$ and a beam spacing of $50''$), was initially used

⁶The National Radio Astronomy Observatory is operated by Associated Universities, Inc., under cooperative agreement with the National Science Foundation.

⁷The Five College Radio Astronomy Observatory is operated with support from the National Science Foundation, and with the permission of the Metropolitan District Commission, Commonwealth of Massachusetts.

for mapping some of the nearest strong sources. We conducted several observing runs at each telescope from 1993 April to 1995 December. Additional observations were conducted remotely at the NRAO 12m telescope in 1997 May and June to confirm some weak detections and to further improve the signal-to-noise ratios for some HCN spectra. The system temperatures at the redshifted HCN line frequencies were typically 220, 250, and 500 K on average on the antenna temperature scales of T_R^* , T_A^* , and T_A^* for the NRAO, IRAM and FCRAO telescopes, respectively. We converted the observed antenna temperature to the main-beam temperature scale (T_{mb}) for all our observations at different telescopes. Table 2 lists various telescope beam efficiencies measured at different telescopes at both the 2.6 and 3.4 mm wavebands. At ~ 3 mm, we adopted the continuum sensitivity (the temperature-to-flux conversion for a point source) on the T_{mb} scale as $S/T_{\text{mb}} = 4.8, 29.0,$ and 23.5 Jy K^{-1} for the IRAM 30m, NRAO 12m, and FCRAO 14m telescopes, respectively.

At the IRAM 30m, we used two 512×1 MHz filter banks and the autocorrelator in its widest bandwidth configuration as back ends. These back ends were connected to three SIS receivers (3mm, 2mm, 1mm) that were usually used to simultaneously observe HCN J=1-0, CS (3-2), and CO J=2-1 lines respectively. The telescope beam diameters (FWHM) for CO J=1-0 and HCN J=1-0 were $22''$ and $27''$, respectively. The NRAO 12m was equipped with dual-polarization 3mm SIS receivers. We connected the dual receivers to a pair of 256×2 MHz filter banks as well as the two 600 MHz wide hybrid spectrometers. The telescope beam diameters (FWHM) for CO J=1-0 and HCN J=1-0 were $55''$ and $72''$, respectively. At the FCRAO 14m, the corresponding back ends for the 15 cooled Schottky diode mixers of the QUARRY array were 15 spectrometers of 64×5 MHz bandwidth. The telescope beam spacing of $50''$ within each row of QUARRY is about the beam size (FWHM) of the 14m telescope at 3 mm.

The IRAM 30m telescope used a wobbling secondary with a beam throw of $\pm 4'$ to achieve flat baselines. Similarly, a nutating subreflector with a chop rate of ~ 1.25 Hz was used at the NRAO 12m together with a position switch (the so-called beam-switch plus position-switch, or “BSP mode”). The beam throws used were in the range of $\pm 2'$ to $\pm 3'$ (the larger beam throw was used for nearest large galaxies with $D_{25} \gtrsim 10'$). Thus, the separations between the OFF reference positions and the ON source position are in the range of $\pm 4'$ to $\pm 6'$. For a couple of the largest galaxies ($D_{25} \gtrsim 20'$) observed at the 12m, we employed position switching in azimuth with offsets comparable to the expected CO source sizes to ensure that the reference positions are completely outside of the sources observed. At the FCRAO 14m, we used double-position switching in azimuth with offsets comparable to the diameters of galaxies. The QUARRY receivers of the FCRAO 14m telescope were efficient in mapping the CO emission in the inner disks of nearby galaxies, but the sensitivity achievable limited our extensive mapping of the weak HCN emission

outside the nuclear regions. No additional beams except for the central beam and sometimes the adjacent two inner beams were detected in HCN with the 14m. Therefore, most of the HCN mapping was eventually conducted with the 12m and 30m telescopes after the initial trial observing runs with the QUARRY at the FCRAO 14m.

We mainly used the IRAM 30m to observe most (rather distant) ULIGs in the sample and to map some nearby starburst galaxies of mostly smaller optical diameters, given the smaller telescope beam compared with the source size and extent for achieving effective mapping. Essentially all other observations were conducted with the NRAO 12m so that one beam measurement covered all emission from relatively distant galaxies including some interacting/merging galaxy pairs. Almost all nearby spiral galaxies were mapped along the major axes with the NRAO 12m. These 12m observations included both the HCN observations initially attempted with the FCRAO 14m QUARRY array, and in several cases, the major axis mapping observations from the IRAM 30m in order to properly compare the total HCN emission estimated with different telescopes (see Table 3). This is essential to better characterize the radial HCN distribution in galaxies (Y. Gao & P.M. Solomon 2004, in preparation).

All observed positions were chosen by checking and comparing the positions of the peak radio continuum emission as determined from the VLA snapshot survey (Condon et al. 1990) or the best positions (with uncertainties $\lesssim 10''$) then listed in the NED.⁸ The observed spectra from all telescopes (except for the FCRAO 14m) were smoothed to ~ 8 MHz resolution, or ~ 20 km s⁻¹ and ~ 27 km s⁻¹ at 2.6 and 3.4mm, respectively. Occasionally, in several of the weakest HCN sources, the spectra were smoothed to 16 MHz to boost the signal-to-noise ratio. Linear baselines were removed from the spectra after emission line windows were chosen to estimate the integrated line intensities. We converted the line temperatures to the main-beam brightness temperature scale T_{mb} (Tables 2 and 3). In many cases, CO lines were also observed from the same telescope for comparison and for determination of the HCN line emission windows. All HCN observations of galaxies so far have shown that the significantly detected HCN line profiles have the same line widths as the CO lines (e.g., Solomon et al. 1992; Helfer & Blitz 1993; Gao 1996). With the CO spectra obtained from the same positions or available in the literature from the same telescope, the integrated line intensities of the weakly detected HCN lines can be more accurately estimated.

Calibrations at all three telescopes were done using the standard chopper wheel method

⁸The NASA/IPAC Extragalactic Database (NED) is operated by the Jet Propulsion Laboratory, California Institute of Technology, under contract with the National Aeronautics and Space Administration.

(Kutner & Ulich 1981). The absolute antenna temperature scale was checked by either observing the standard calibration sources or by the measured CO line strengths of the targets (mostly for the nearest strong sources) as compared with the standard spectra at the telescopes and the known CO spectra available in the literature. Pointing was checked by observing quasars or planets about every 2–3 hours, with typical errors of $\sim 3''$ for the IRAM 30m, and $\sim 5'' - 10''$ for the NRAO 12m and the FCRAO 14m. Focus was also monitored a few times per day mostly using planets. More detailed discussions of the observations and the antenna temperature scales at different telescopes can be found in Gao (1996, 1997).

4. RESULTS AND DISCUSSION

4.1. Spectra

We present all HCN spectra in Figs. 2 and 3 for the IRAM 30m and the NRAO 12m telescopes, respectively, including a few weak ($\sim 3\sigma$) detections. For most galaxies, we also show the CO spectra taken at the same position from the same telescope for comparison. A few CO spectra in Figure 2, however, are CO J=2-1 lines, which have much smaller beam sizes compared with that of the HCN J=1-0 spectra. In some cases, the velocity range of CO emission, obtained from the published CO spectra in the literature with the same telescopes or comparable telescope beam sizes, is indicated instead. NGC 253, NGC 2903, M82, and NGC 6946 were mapped by both the IRAM 30m and the NRAO 12m and therefore appear in both Figs. 2 and 3. Only the central HCN spectra of those nearby galaxies highlighted in Table 1 are displayed here; the detailed HCN mapping will be shown in a future paper (Y. Gao & P.M. Solomon 2004, in preparation).

We detected HCN emission in essentially all of the sources (except NGC 1055) listed in Table 1, though a few galaxies were only marginally detected. The observed line intensities (of both HCN and CO if applicable) are listed in Table 3 together with other measured quantities useful for analysis. The derived global properties of the line luminosities and their ratios using methods discussed below (§4.2) are listed in Table 4.

Fully sampled mapping is essential in order to estimate the total HCN emission in large spiral galaxies (Gao 1996, 1997; Y. Gao & P.M. Solomon 2004, in preparation) because a substantial fraction of the total HCN emission is distributed outside the ~ 1 kpc nuclear regions (which are covered by the central beams in these observations). Therefore, we did not add more nearby galaxies with HCN detections from their centers from the literature into our HCN sample. Those data only measure lower limits to the HCN luminosity since

only the central beam detections were made for these nearby large spiral galaxies, and the HCN emission outside the central ~ 1 kpc nuclear regions is unknown. Notice that about 15% of the galaxies in our HCN survey sample also have either upper or lower limits in the total HCN emission or luminosity (Tables 3 & 4). The upper limits in the HCN measurements correspond to weak detections ($\sim 3\sigma$) or non-detections ($\lesssim 2\sigma$, only for NGC 1055) or to nearby galaxies with good detections in the center but with only weak detections or non-detections at the off-center positions. The lower limits in the HCN luminosity are for a few nearby galaxies with good HCN detections from the galaxy centers, but no systematic mapping or detections at off-center positions (NGC 2903 is exceptional since it was mapped with the IRAM 30m, yet more sensitive and extensive mapping is still required to estimate the total HCN emission). This is similar to the case of more than a dozen nearby galaxies with only central beam HCN observations in the literature (thus lower limits to the total HCN emission). We include our own limits, but not the HCN limits in the literature in the final HCN sample.

4.2. HCN and CO Line Luminosities

For sources much smaller than the telescope beam, the HCN luminosity is calculated using

$$L'_{\text{HCN}} = \int T_{\text{b}}(\text{HCN}) dV d\Omega_{\text{s}} d_A^2 \approx \pi/(4\ln 2) \theta_{\text{mb}}^2 I_{\text{HCN}} d_L^2 (1+z)^{-3} \quad (1)$$

(see Solomon et al. 1997 for details, L' with a unit of $\text{K km s}^{-1} \text{ pc}^2$ is introduced to distinguish it from normal L , which has proper power units), where Ω_{s} is the solid angle subtended by the source area,

$$I_{\text{HCN}} = \int T_{\text{mb}}(\text{HCN}) dV = \int T_{\text{b}}(\text{HCN}) dV d\Omega_{\text{s}} / [(1+z)\Omega_{\text{s}*\text{b}}] \quad (2)$$

is the observed integrated line intensity (as converted to the beam-diluted main-beam temperature scale), $T_{\text{b}}(\text{HCN})$ is the intrinsic source brightness temperature, $\Omega_{\text{s}*\text{b}} \approx \pi/(4\ln 2) \theta_{\text{mb}}^2$ is the solid angle of the source convolved with the diameter (FWHM) of the telescope Gaussian beam θ_{mb} , and d_L and d_A are the luminosity distance⁹ and the angular size distance to the source, respectively, related by $d_L = d_A(1+z)^2 = 7994.5[1+z - (1+z)^{1/2}] \text{ Mpc}$.

For large galaxies where HCN was observed at several positions along the major axis,

⁹ $H_0=75\text{km s}^{-1} \text{ Mpc}^{-1}$ and $q_0 = 0.5$ were used in this paper

the total integrated HCN flux over the source,

$$F_{\text{HCN}} = \int T_{\text{mb}}(\text{HCN}) dV d\Omega_{\text{s*b}}, \quad (3)$$

is estimated following the empirical formula adopted in Solomon & Sage (1988; also Sage 1987) to calculate the total CO emission. The total HCN emission is obtained by summing all the measured line fluxes along the major axes with weights determined from considerations of θ_{mb} , the (source) disk size, D_{25} , and the disk inclination, and assumption of an axisymmetric source distribution. Thus, for nearby galaxies,

$$L'_{\text{HCN}} = \int T_{\text{mb}}(\text{HCN}) dV d\Omega_{\text{s*b}} d_A^2 (1+z) = F_{\text{HCN}} d_L^2 (1+z)^{-3}. \quad (4)$$

The CO luminosity is calculated similarly with the same formula listed above (switching HCN with CO). For brevity, we hereafter use the symbol L rather than L' for the line luminosity in unit of $\text{K km s}^{-1} \text{ pc}^2$ for both CO and HCN emission.

For those nearby galaxies that we observed with different telescopes, the agreement in the estimated total HCN fluxes is rather good (Table 3), given the weak HCN lines detected outside the nuclear regions in most cases. For all positions observed in HCN, the permitted velocity ranges are available either from our own, or published, CO observations. As discussed in § 3, the weak detections or upper limits for the HCN line intensities can be better estimated when the HCN line emission windows are known/assumed from the CO lines, and thus the HCN results are rather robust. The uncertainties in the total HCN (and occasionally CO) luminosities are up to $\sim 50\%$ including the calibration errors of different telescopes, but in most cases only $\sim 30\%$ or better. The largest uncertainties are only present in a few galaxies with the marginal detections ($\sim 3\sigma$) and in some nearby large galaxies with very limited points observed where extensive mapping along their major axes is still required for more accurate estimates of the total HCN emission.

4.3. Correlation between HCN and IR Emission

Figure 4 shows a tight linear correlation between L_{HCN} and L_{IR} over 3 orders of magnitude in IR luminosity. The originally proposed correlation, based on 10 representative galaxies (Solomon et al. 1992), is also noted for comparison. We recalculated L_{HCN} , L_{CO} (see §4.2) based on the measured line intensities I_{HCN} and I_{CO} listed in Table 1 of Solomon et al. (1992). Obviously, the new HCN data from a sample more than 5 times larger closely follow the trend established by Solomon et al. (1992) and have about the same scatters. A least-squares fit including published data (almost entirely from Solomon

et al. 1992), yet excluding our HCN limits, yields a slope of 1.00 ± 0.05 , with a correlation coefficient $R=0.94$ ($R^2 = 0.88$). The correlation implies $\log L_{\text{IR}} = 1.00 \log L_{\text{HCN}} + 2.9$. When we include all galaxies in the fit and take the limits given in Table 4 as the HCN luminosities, the linear relation remains almost the same with $\log L_{\text{IR}} = 0.97 \log L_{\text{HCN}} + 3.1$ and the same correlation coefficient.

We have therefore confirmed the tight correlation between IR and HCN luminosities in a large, statistically significant sample. LIGs/ULIGs have the highest L_{HCN} and highest ratio of $L_{\text{HCN}}/L_{\text{CO}}$, and many of them have L_{HCN} even larger than L_{CO} of the Milky Way, which implies a relatively high fraction of dense molecular gas as well as an extremely large reservoir of dense molecular gas (discussed further in § 4.5). The detailed discussion of the tight correlation between L_{IR} and L_{HCN} and other relationships, as well as their implications, will be fully explored in Paper II. In this paper, we would like to show that HCN emission is indeed a good tracer of dense molecular gas (in the next two sections). Therefore, the tight correlation between far-IR and HCN suggests that active star formation is strongly related to the mass of dense molecular gas and the main source of the strong IR emission in LIGs/ULIGs is mostly from active star formation.

In Figure 5, we have divided the sample into two subsamples: LIGs and ULIGs with $L_{\text{IR}} \geq 10^{11} L_{\odot}$ are plotted as filled circles, and less luminous galaxies are shown as open circles. Apparently, all LIGs/ULIGs have L_{HCN} larger than $10^8 \text{ K km s}^{-1} \text{ pc}^2$, whereas the less luminous normal spiral galaxies have $L_{\text{HCN}} \lesssim 10^8 \text{ K km s}^{-1} \text{ pc}^2$. We also note that several ULIGs have $L_{\text{HCN}}/L_{\text{CO}}$ as high as ~ 0.25 , whereas most normal galaxies have $L_{\text{HCN}}/L_{\text{CO}}$ nearly 10 times smaller. Other systematic differences between these two subsamples can also be easily seen in various other correlations presented in Paper II.

4.4. Excitation of HCN

We here try to empirically demonstrate that the radiative pumping, or populating, of the $J=1$ level of HCN through a vibrational transition at $14 \mu\text{m}$ wavelength, does not enhance significantly the excitation of the HCN $J=1-0$ emission. Since the mid-IR vibrational transition of HCN falls within the *IRAS* $12 \mu\text{m}$ bandpass and there are no other direct measurements of the $14 \mu\text{m}$ emission available, we use the $12 \mu\text{m}$ flux as an approximation. We show in Figure 5 two correlation plots that involve the *IRAS* $12 \mu\text{m}$ emission to illustrate that the enhancement in the excitation of HCN through a vibrational transition, by this potential mid-IR radiative pumping, as postulated by Aalto et al. (1995), is not important. Previous HCN modeling also found that the radiative pumping from the dust continuum emission has little effect on the excitation of the rotational transitions in

the vibrational ground state of HCN (e.g., Stutzki et al. 1988; Paglione, Jackson, & Ishizuki 1997).

Although there is still a good correlation between the 12 μm and HCN emission (a squared correlation coefficient of $R^2 = 0.75$), the relationship is not particularly strong as compared with the much tighter correlation between IR and HCN emission (Fig. 4, $R^2 = 0.88$). In fact, the correlation between the 12 μm and HCN emission appears to be the weakest among the correlations between the four *IRAS* waveband and HCN emission. Both the 60 and 100 μm luminosities correlate much better with the HCN luminosity. For example, the correlation between 100 μm and HCN emission ($R^2 = 0.89$) is significantly better than that between 12 μm and HCN emission ($R^2 = 0.75$). A three-parameter fit of HCN emission as a function of both 12 μm and 100 μm emission clearly shows that most of the contribution to the fit is from the 100 μm emission alone, whereas there is little from the 12 μm emission. Should the mid-IR pumping be an important effect in the excitation of HCN in the vibrational ground state of HCN, a tighter correlation between the 12 μm and HCN luminosities than any correlations between the HCN and 60 μm , 100 μm , and total IR luminosities would be expected. We observe the contrary.

We can also use the luminosity ratio, rather than the single luminosity alone, to normalize the correlations in order to eliminate the distance and galaxy size dependencies inherent in the luminosity correlations (more examples are in Paper II). There is only a weak correlation between $L_{12\mu\text{m}}/L_{\text{CO}}$ and $L_{\text{HCN}}/L_{\text{CO}}$ ($R^2 = 0.29$), whereas the correlation between $L_{100\mu\text{m}}/L_{\text{CO}}$ and $L_{\text{HCN}}/L_{\text{CO}}$ is still fairly strong ($R^2 = 0.56$). Clearly, these results suggest that the mid-IR emission is only loosely correlated with the HCN emission, and the correlation between the far-IR emission and the HCN emission is significantly tighter in comparison. This essentially rules out the possibility that the mid-IR pumping in the vibrational ground state of HCN could be one of the significant contributors to the HCN J=1-0 emissivity.

To strengthen these results, we compare the HCN luminosity and the ratio of HCN and CO luminosities ($L_{\text{HCN}}/L_{\text{CO}}$) with the excess 12 μm emission estimated by either the ratio of 12 μm and total IR or the ratio of 12 μm and 100 μm (or 12 μm and 60 μm) luminosities. We plot the luminosity ratio of $L_{12\mu\text{m}}/L_{\text{IR}}$ versus L_{HCN} in Figure 5a and the luminosity ratios of $L_{\text{HCN}}/L_{\text{CO}}$ versus $L_{12\mu\text{m}}/L_{100\mu\text{m}}$ in Figure 5b. Obviously, no correlations are observed in these plots and there is no sign of increased HCN emission or an increased $L_{\text{HCN}}/L_{\text{CO}}$ ratio for galaxies with a 12 μm emission excess. Similar plots for relationships between the luminosity ratios of $L_{\text{HCN}}/L_{\text{CO}}$ and $L_{12\mu\text{m}}/L_{\text{IR}}$ or between $L_{\text{HCN}}/L_{\text{CO}}$ and $L_{12\mu\text{m}}/L_{60\mu\text{m}}$ show no correlations either. Therefore, there is little evidence for a direct connection between the 12 μm and HCN emission, even for galaxies with excessive 12 μm

emission (Fig. 5). The contribution of mid-IR radiative pumping to the HCN excitation must be negligible when it is compared to the collisional excitation by dense molecular hydrogen (see § 4.5).

Gao & Solomon (Paper II) show that L_{HCN} can be quite accurately predicted from the IR (or far-IR) and CO luminosities. In this three-parameter model fit, L_{IR} appears to be slightly more important, but L_{CO} is also a significant predictor for L_{HCN} [the HCN(L_{IR} , L_{CO}) model (see § 3.3.1 and Table 3 in Paper II)]. Here we can add $L_{12\mu\text{m}}$ as an additional parameter into the model fit for L_{HCN} to check whether $L_{12\mu\text{m}}$ is a non-negligible predictor for L_{HCN} as well. This could test the significance of the mid-IR emission contribution to HCN as compared with that of the far-IR and CO emission. We find that the model fit changes only marginally with no improvement in the correlation coefficient or the rms scatter of the fit. In fact, no difference is noticeable in the model fit whether $L_{12\mu\text{m}}$ is added or not. Therefore, even though there exists a correlation between $12\mu\text{m}$ and HCN emission, the correlation is significantly worse than the correlations between the HCN and IR emission of three other *IRAS* bands, and the contribution to HCN from $12\mu\text{m}$ emission is negligible. We conclude that there is no clear evidence to claim that the mid-IR pumping can significantly enhance the HCN emission.

For the archetypal AGN/starburst hybrid galaxy NGC 1068, which has the strongest mid-IR emission in our HCN sample, the $L_{\text{HCN}}/L_{\text{CO}}$ ratio is also one of the highest. In particular, a very high HCN/CO ratio ($\gtrsim 0.3$) within ~ 100 pc nuclear region is observed (Jackson et al. 1993; Tacconi et al. 1994; Helfer & Blitz 1995) in the interferometric maps, which appears to be the mid-IR compact core around AGN (Le Floc’h et al. 2001). Is this an example that the mid-IR pumping has significantly enhanced the global HCN emission? Apparently not, since the innermost $\lesssim 100$ pc nuclear region around the AGN contributes little to the average HCN/CO ratios in the circumnuclear (~ 0.5 – 1 kpc) starburst ring where most of molecular gas is located. Also in NGC 1068, the ratio $f_{12\mu\text{m}}/f_{100\mu\text{m}} = 0.16$ is much higher than in any other galaxy in the sample. Yet, it is still not certain whether the extreme excess of the mid-IR emission contributes significantly to the excitation of HCN. This is because galaxies with the lowest $L_{12\mu\text{m}}/L_{\text{IR}}$ ratios can have even larger HCN luminosities than NGC 1068 (Fig. 5a) and galaxies with the lowest $f_{12\mu\text{m}}/f_{100\mu\text{m}}$ ratios appear to have similar or even higher $L_{\text{HCN}}/L_{\text{CO}}$ ratios than NGC 1068 (Fig. 5b). Thus, globally the high $L_{\text{HCN}}/L_{\text{CO}}$ ratio and high L_{HCN} in galaxies may have nothing to do with the mid-IR emission excess. Again, there is no indication that the strong mid-IR emission is linked to the high ratio of HCN/CO or large HCN luminosity even for galaxies with the most extreme mid-IR emission excesses.

4.5. Mass of Dense Molecular Gas Traced by HCN

The mass of molecular gas in galaxies is typically derived from the CO luminosity using the “standard” CO-to-H₂ conversion factor

$$M(H_2) = 4.78 L_{CO} M_{\odot} (\text{K km s}^{-1} \text{ pc}^2)^{-1} \quad (5)$$

(e.g., Solomon & Barrett 1991; Young & Scoville 1991 and references therein), estimated from the Galactic disk GMCs in the Milky Way. Although this conversion corresponds to $N(H_2)/I_{CO} = 3 \times 10^{20} \text{ cm}^{-2} (\text{K km s}^{-1})^{-1}$, rather than the recent calibration of $N(H_2)/I_{CO} = 1.7 \times 10^{20} \text{ cm}^{-2} (\text{K km s}^{-1})^{-1}$ (Dame et al. 2001; Hunter et al. 1997), we use it simply for easy comparison with previous CO studies of galaxies. As discussed in Downes, Solomon, & Radford (1993), Solomon et al. (1997), and Downes & Solomon (1998), however, we caution that it might overestimate the molecular gas mass in ULIGs by factors of 3–5. Unlike normal spiral galaxies, where a large fraction of CO emission comes mainly from GMCs distributed in the inner disk, the CO distribution in ULIGs is extremely concentrated in the nuclear regions and may fill the entire volume since even the intercloud medium may be molecular (Solomon et al. 1997; Downes & Solomon 1998). High-resolution CO imaging of ULIGs has indeed shown extremely high concentration of CO emission in the central few hundred parsecs (e.g., Downes & Solomon 1998). For ULIGs, the conversion factor is thus lower than for normal spiral galaxies. Nevertheless, we still adopt the standard CO-to-H₂ gas mass conversion (eq. [5]) for convenience since 90% of the galaxies in our sample are not ULIGs. The ratio of $L_{IR}/M(H_2)$, often referred to as the star formation efficiency, is also listed in Table 4.

Observations of H¹³CN (Nguyen-Q-Rieu et al. 1992; Wild et al. 1992) indicate that extragalactic HCN emission is also optically thick, just like CO emission. The conversion factor between HCN and the mass of the dense molecular gas, however, is poorly constrained as there is no direct calibration from GMCs or GMC core regions in the disk of the Milky Way. From observations of higher transition CS emission, Plume et al. (1997) find a typical GMC core has a diameter of 1 pc and mass of 3800M_⊙. Then the rms velocity of a virialized cloud with these parameters is $\sim 5 \text{ km s}^{-1}$, consistent with the observed FWHM line width. We have carried out large velocity gradient (LVG) calculations that include radiative trapping for HCN J=1-0 to determine the mass of dense molecular gas from the measured HCN brightness temperatures (e.g., Kwan & Scoville 1975), using the collision rates given by Green & Thaddeus (1974). For an HCN abundance (relative to H₂) of 2×10^{-8} (e.g., Irvine, Goldsmith, & Hjalmarsen 1987; Lahuis & van Dishoeck 2000) and a velocity gradient of $\sim 5 \text{ km s}^{-1} \text{ pc}^{-1}$, this gives $[\text{HCN}]/(dv/dr) \sim 4 \times 10^{-9} (\text{km s}^{-1} \text{ pc}^{-1})^{-1}$. For a kinetic temperature of 20–50 K and the intrinsic HCN line brightness temperature

$T_b > 5$ K, this gives $N(H_2)/I_{\text{HCN}} \lesssim 2 \times 10^{21} \text{ cm}^{-2} (\text{K km s}^{-1})^{-1}$ or

$$M_{\text{dense}}(H_2) \lesssim 25 L_{\text{HCN}} M_{\odot} (\text{K km s}^{-1} \text{ pc}^2)^{-1} \quad (6)$$

for H_2 at a density $\gtrsim 10^4/\tau \text{ cm}^{-3}$, where $M_{\text{dense}}(H_2)$ means the dense molecular gas as traced by HCN emission, and $\tau \gtrsim 1$ is the optical depth of the HCN J=1-0 line.

For higher intrinsic HCN line brightness temperature $T_b > 15$ K, higher gas density $n(H_2) \gtrsim 3 \times 10^4/\tau \text{ cm}^{-3}$, and the same abundance and velocity gradient, however, LVG results give $N(H_2)/I_{\text{HCN}} \lesssim 1.3 \times 10^{21} \text{ cm}^{-2} (\text{K km s}^{-1})^{-1}$, or

$$M_{\text{dense}}(H_2) \lesssim 15 L_{\text{HCN}} M_{\odot} (\text{K km s}^{-1} \text{ pc}^2)^{-1}. \quad (7)$$

Alternatively, for a virialized cloud core of an average density $\langle n(H_2) \rangle = 3 \times 10^4 \text{ cm}^{-3}$ and $T_b \sim 35$ K (e.g., Radford, Solomon, & Downes 1991),

$$M_{\text{dense}}(H_2) \approx 2.1 \frac{\langle n(H_2) \rangle^{1/2}}{T_b} L_{\text{HCN}} \sim 10 L_{\text{HCN}} M_{\odot} (\text{K km s}^{-1} \text{ pc}^2)^{-1}, \quad (8)$$

almost same as that obtained from LVG approximation (eq. [7]).

The LVG calculations above give perhaps an upper limit for the conversion factor between HCN and the mass of dense molecular gas (cf. Mauersberger & Henkel 1993) since the much lower intrinsic HCN line brightness temperature $T_b > 5$ or 15 K was used besides other approximations in the LVG estimates. Higher T_b indeed tends to result in a smaller conversion factor allowed by LVG (eq. [7]). HCN hot cores in regions of massive star formation usually have extremely high temperature up to hundreds of degrees (e.g., Boonman et al. 2001). Thus, it is likely that a much smaller conversion factor holds under these extreme conditions. Moreover, there are some other mechanisms possible to help excite HCN molecule, e.g., excess HCN abundance (Bergin, Snell, & Goldsmith 1996; Lahuis & van Dishoeck 2000) resulting from the active star-forming environment and high supernovae events, and collisions with electrons. Although these are most likely insignificant (e.g., mid-IR radiative pumping discussed in previous section) and the dominant mechanism should still be collisions with molecular hydrogen, they could work collectively to lower the conversion factor given in equations (6) and (7). Other constraints such as the total molecular gas mass estimated from the CO observations, the higher frequency CO line observations, and the dynamical mass estimations (e.g., Solomon et al. 1997; Downes & Solomon 1998), all seem to point to a smaller conversion factor, particularly for LIGs/ULIGs. Thus, a lower conversion factor given in equation (8) is more likely.

In fact, since the luminosity ratio $L_{\text{HCN}}/L_{\text{CO}}$ in ULIGs can be as large as $\sim 25\%$ (e.g., Mrk 231, Mrk 273 and *IRAS* 17208-0014), the true conversion factor between HCN and the mass of dense molecular gas should obviously be much smaller than the upper limit allowed by the LVG calculation (eq. [7]) in order to reconcile with the total molecular gas mass estimated from the standard CO-to-H₂ conversion (eq. [5]). Particularly for ULIGs, even equation (8) might still overestimate the dense molecular gas mass since T_b could be indeed very high ($\gtrsim 50$ K) and the standard CO-to-H₂ conversion of equation (5) should be reduced by a factor of 5 in ULIGs (Downes & Solomon 1998). The main difference between normal spiral galaxies and ULIGs in the HCN-to-H₂ conversion, however, is the drastically different molecular line brightness temperatures. While $T_b \sim 10$ K is valid for most normal spiral galaxies, a factor of 5 higher $T_b \sim 50$ K was deduced for ULIGs undergoing extreme starbursts (Downes & Solomon 1998), which argues for a much lower HCN-to-H₂ conversion factor than those given in the above equations.

Nevertheless, this also indicates that ULIGs with the highest $L_{\text{HCN}}/L_{\text{CO}}$ ratio are likely to have most ($\gtrsim 50\%$) of their molecular gas at high density ($\gtrsim 3 \times 10^4/\tau \text{ cm}^{-3}$) and that $L_{\text{HCN}}/L_{\text{CO}}$ ratio can indeed be used as an indicator of the fraction of dense molecular gas in galaxies. On the other hand, $L_{\text{HCN}}/L_{\text{CO}}$ ratio also indicates the average molecular gas density in galaxies. Given the large uncertainty of the HCN-to-H₂ conversion, the same as is true for CO-to-H₂ conversion, we suggest that a conversion factor of $M_{\text{dense}}(\text{H}_2)/L_{\text{HCN}} \sim 10 \text{ M}_\odot (\text{K km s}^{-1} \text{ pc}^2)^{-1}$ (eq. [8]) is the more reasonable one to use, and we adopt this relation to estimate the total dense molecular gas mass in galaxies as tabulated for $L_{\text{IR}}/M_{\text{dense}}(\text{H}_2)$ in Table 4. Accurate determination of the conversion factor between HCN and the mass of dense molecular gas needs further extensive studies including higher frequency HCN observations (e.g., Jackson et al. 1995; Paglione et al. 1997) and more detailed modeling.

5. CONCLUSIONS

We present systematic HCN J=1-0 observations (complemented with CO observations) of a sample of 53 IR/CO-bright and/or luminous galaxies, which is the largest HCN sample and most sensitive HCN survey of external galaxies so far. Ultraluminous infrared galaxies have the highest HCN luminosities, usually several times larger than the CO luminosity of our own Galaxy. Many luminous infrared galaxies have HCN luminosities comparable to the CO luminosity of the Galaxy. The ratio of HCN and CO luminosities can be as large as $\sim 25\%$ in ultraluminous infrared galaxies, nearly an order of magnitude higher than most normal spiral galaxies.

We compared the HCN line emission with the far-IR emission (an indicator of the rate of high-mass OB star formation). All galaxies surveyed follow the tight correlation between IR and HCN luminosities initially proposed by Solomon et al. (1992). Since stars form only in dense clouds and the HCN-emitting gas (i.e., the dense molecular gas) and IR emission appear closely and physically related, then active star formation is the dominant source of IR emission in luminous and ultraluminous galaxies. This is fully discussed in Paper II.

There is no particularly strong correlation between the 12 μm and HCN luminosities. The correlations between 100 μm (and 60 μm) and HCN emission are much better correlated in comparison. Galaxies with excess 12 μm emission do not show stronger HCN emission or higher HCN/CO luminosity ratios. Thus, mid-IR radiative pumping of HCN excitation is of little significance when compared with the collisional excitation by dense molecular gas.

We also discussed the use of HCN J=1-0 emission as a tracer of higher density molecular gas ($\gtrsim 3 \times 10^4/\tau \text{ cm}^{-3}$) and adopted a HCN-to- H_2 conversion factor $M_{\text{dense}}(\text{H}_2)/L_{\text{HCN}} \sim 10 M_{\odot} (\text{K km s}^{-1} \text{ pc}^2)^{-1}$. Luminous and ultraluminous infrared galaxies usually have much higher HCN brightness temperature, which might result in a lower conversion factor. Analyses including LVG calculations indicate that the HCN luminosity measures the mass of dense molecular gas and the HCN/CO luminosity ratio indicates the fraction of molecular gas in a dense phase.

We thank Simon Radford, Dennis Downes, and Mark Heyer for help with some of the observations. We appreciate the generous support and allocation of observing time from the NRAO 12m, the IRAM 30m, and the FCRAO 14m. We would also like to acknowledge Edwin Bergin, Paul Goldsmith, and Ron Snell for providing their LVG code. The careful review and helpful comments of the anonymous referee are greatly acknowledged. This research has made use of the NASA/IPAC Extragalactic Database (NED) which is operated by the Jet Propulsion Laboratory, Caltech, under contract with the National Aeronautics and Space Administration.

REFERENCES

- Aalto, S., Booth, R.S., Black, J.H., & Johansson, L.E.B. 1995, *A&A*, 300, 369
- Bally, J., Stark, A.A., Wilson, R.W., & Henkel, C. 1987, *ApJS*, 65, 13
- Bally, J., Stark, A.A., Wilson, R.W., & Henkel, C. 1988, *ApJ*, 324, 223
- Bergin, E.A., Snell, R.L., & Goldsmith, P.F. 1996, *ApJ*, 460, 343
- Boonman, A.M.S., Stark, R., van der Tak, E.F.S. et al. 2001, *ApJ*, 553, L63
- Brouillet, N., & Schilke, P. 1993, *A&A*, 277, 381
- Carlstrom, J.E. 1988, in *Galactic and Extragalactic Star Formation*, ed. R.E. Rudritz, & M. Fich (Dordrecht: Reidel), 571
- Carlstrom, J.E., Jackson, J., Ho, P.T.P., & Turner, J.L. 1990, in *The Interstellar Medium in External Galaxies*, eds. D.J. Hollenbach & H.A. Thornson (Washington, DC: NASA CP 3084), 337
- Condon, J.J., Helou, G., Sanders, D.B., & Soifer, B.T. 1990, *ApJS*, 73, 359
- Curran, S.J., Aalto, S., & Booth, R.S. 2000, *A&AS*, 141, 193
- Dame, T.M., Hartmann, D., & Thaddeus, P. 2001, *ApJ*, 555, 487
- Downes, D., Radford, S.J.E., Guilloteau, S., et al. 1992, *A&A*, 262, 424
- Downes, D., Solomon, P.M., & Radford, S.J.E. 1993, *ApJ*, 414, L13
- Downes, D., & Solomon, P.M. 1998, *ApJ*, 507, 615
- Gao, Y. 1996, Ph.D. thesis, SUNY at Stony Brook
- Gao, Y. 1997, *PASP*, 109, 1189
- Gao, Y., & Solomon, P.M. 2004, *ApJ*, 606, May 1 (Paper II, astro-ph/0310339)
- Green, S., & Thaddeus, P. 1974, *ApJ*, 191, 653
- Helfer, T.T., & Blitz, L. 1993, *ApJ*, 419, 86
- Helfer, T.T., & Blitz, L. 1995, *ApJ*, 450, 90
- Helfer, T.T., & Blitz, L. 1997a, *ApJ*, 478, 162
- Helfer, T.T., & Blitz, L. 1997b, *ApJ*, 478, 233
- Henkel, C., Whiteoak, J.B., Nyman, L.-Å., & Harju, J. 1990, *A&A*, 230, L5
- Horellou, C., Casoli, F., Combes, F., & Dupraz, C. 1995, *A&A*, 298, 743
- Hunter, S.D., et al. 1997, *ApJ*, 481, 205

- Irvine, W.M., Goldsmith, P.F., & Hjalmarsen, Å. 1987, in *Interstellar Processes*, eds. D.J. Hollenbach & H.A. Thronson, Jr. (Dordrecht: Reidel), 561
- Israel, F.P. 1992, *A&A*, 265, 487
- Jackson, J.M., Eckart, A., Cameron, M., Wild, W., Ho, P.T.P., Pogge, R.W., & Harris, A.I. 1991, *ApJ*, 375, 105
- Jackson, J.M., Paglione, T.A.D., Ishizuki, S., & Nguyen-Q-Rieu. 1993, *ApJ*, 418, L13
- Jackson, J.M., Paglione, T.A.D., Carlstrom, J.E., & Nguyen-Q-Rieu. 1995, *ApJ*, 438, 695
- Jackson, J.M., Heyer, M.H., Paglione, T.A.D., & Bolatto, A.D. 1996, *ApJ*, 456, L91
- Kohno, K., Kawabe, R., & Vila-Vilaro, B. 1999, *ApJ*, 511, 157
- Kohno, K., Kawabe, R., Tosaki, T., & Okumura, S.K. 1996, *ApJ*, 461, L29
- Kuno, N., Nakai, N., Sorai, K. et al. 2002, *PASJ*, 54, 555
- Kutner, M., & Ulich, B. 1981, *ApJ*, 250, 341
- Kwan, J., & Scoville, N.Z. 1975, *ApJ*, 195, L85
- Lada, E.A., Bally, J., & Stark, A.A. 1991, *ApJ*, 368, 432
- Lahuis, F., & van Dishoeck, E.F. 2000, *A&A*, 355, 699
- Le Flo'ch, E., Mirabel, I.F., Laurent, O., Charmandaris, V., Gallais, P., Sauvage, M., Vigroux, L., & Cesarsky, C. 2001, *A&A*, 367, 487
- Lee, Y., Snell, R.L., & Dickman, R.L. 1990, *ApJ*, 355, 536
- Lee, C.W. 1996, *ApJS*, 105, 129
- Mauersberger, R., & Henkel, C. 1989, *A&A*, 223, 79
- Mauersberger, R., & Henkel, C. 1993, *Rev. Modern Astron.*, 6, 69
- Mauersberger, R., Henkel, C., Wilson, T.L., & Harju, J. 1989, *A&A*, 226, L5
- McQuinn, K.B.W., Simon, R., Law, C.J. et al. 2002, *ApJ*, 576, 274
- Nguyen-Q-Rieu, Nakai, N. & Jackson, J.M. 1989 *A&A*, 220, 57
- Nguyen-Q-Rieu, Jackson, J.M., Henkel, C., Truon-Bach & Mauersberger, R. 1992, *ApJ*, 399, 521
- Paglione, T.A.D., Jackson, J.M., Ishizuki, S., & Nguyen-Q-Rieu 1995a, *AJ*, 109, 1716
- Paglione, T.A.D., Tosaki, T., & Jackson, J.M. 1995b, *ApJ*, 454, L117
- Paglione, T.A.D., Jackson, J.M., & Ishizuki, S. 1997, *ApJ*, 484, 656
- Paglione, T.A.D., Jackson, J.M., Bolatto, A.D., & Heyer, M.H. 1998, *ApJ*, 493, 680

- Peng, R., Zhou, S., Whiteoak, J.B., Lo, K.Y., & Sutton, E.C. 1996, ApJ, 470, 821
- Plume, R., Jaffe, D.T., Evans, N.J., II, et al. 1997, ApJ, 476, 730
- Radford, S.J.E., Delannoy, J., Downes, D., et al. 1991, in IAU Symp 146, *Dynamics of Galaxies and their Molecular Cloud Distributions*, ed. F. Combes, & F. Casoli (Dordrecht: Kluwer), 303
- Radford, S.J.E., Solomon, P.M., & Downes, D. 1991, ApJ, 368, L15
- Reynaud, D. & Downes, D. 1997, A&A, 319, 737
- Rice, W., Lonsdale, C.J., Soifer, B.T., et al. 1988, ApJS, 68, 91
- Sage, L.J. 1987, Ph.D. thesis, SUNY Stony Brook
- Sage, L.J., Shore, N., & Solomon, P.M. 1990, ApJ, 351, 422
- Sanders, D.B., Mazzarella, J.M., Kim, D.-C., Surace, J.A., & Soifer, B.T. 2003, AJ, 126, 1607
- Sanders, D.B., Scoville, N.Z., & Soifer, B.T. 1991, ApJ, 370, 158
- Sanders, D.B., & Mirabel, I.F. 1996, ARA&A, 34, 749
- Sandqvist, A., Jörsäter, S., & Lindblad, P.O. 1995, A&A, 295, 585
- Shen, J. & Lo, K.Y. 1995, ApJ, 445, L99
- Shibatsuka, T., Matsushita, S., Kohno, K., & Kawabe, R. 2003, PASJ, 55, 87
- Solomon, P.M., & Barrett, J.W. 1991, in *Dynamics of Galaxies and their Molecular Cloud Distributions*, ed. Combes, F., & Casoli, F. (Dordrecht: Kluwer) p. 235
- Solomon, P.M., Downes, D. & Radford, S.J.E. 1992, ApJ, 387, L55
- Solomon, P.M., Downes, D., Radford, S.J.E., & Barrett, J.W. 1997, ApJ, 478, 144
- Solomon, P.M., Radford, S.J.E., & Downes, D. 1990, ApJ, 348, L53
- Solomon, P.M. & Sage, L.J. 1988, ApJ, 334, 613
- Sorai, K., Nakai, N., Kuno, N., & Nishiyama, K. 2002, PASJ, 54, 179
- Strauss, M.A., Huchra, J.P., Davis, M., Yahil, A., Fisher, K.B. & Tonry, J. 1992, ApJS, 83, 29
- Stutzki, J., Genzel, R., Harris, A.I., Herman, J., & Jaffe, D.T. 1988, 330, L125
- Tacconi, L.J., Genzel, R., Blietz, M., Cameron, M., Harris, A. & Madden, S. 1994, ApJ, 426, L77
- Tinney, C.G., Scoville, N.Z., Sanders, D.B. & Soifer, B.T. 1990, ApJ, 362, 473
- Wild, W., & Eckart, A. 2000, A&A, 359, 483

- Wild, W., Harris, A.I., Eckart, A., et al. 1992, A&A, 265, 447
- Xie, S., Young, J.S., & Schloerb, F.P. 1994, ApJ, 421, 434
- Young, J.S., Kenney, J.D., Tacconi, L. et al. 1986, ApJ, 311, L17
- Young, J.S., Xie, S., Kenney, J.D.P., & Rice, W.L. 1989, ApJS, 70, 699
- Young, J.S., & Scoville, N.Z. 1991, ARA&A, 29, 581
- Young, J.S., Xie, S., Tacconi, L., et al. 1995, ApJS, 98, 219

TABLE 1. HCN Survey Source List and Galaxy Properties

Galaxies ^a	R.A. (1950)	DEC.	$V(\text{km s}^{-1})^b$	$d(\text{Mpc})^c$	$D_{25} (')$	P.A. ^d	Inclination	Classifications ^e
NGC 253	00 ^h 45 ^m 05 ^s .9	−25°33′40″	251	2.5	27.5	51°	76°	SAB(s)c,HII
IC 1623	01 05 19.5	−17 46 26	6028	81.7	0.4	GPair:pec
NGC 660	01 40 20.7	13 23 32	856	14.0	8.3	170	67	SB(s)a:pec,HII,LINER
NGC 695	01 48 27.8	22 20 07	9769	133.5	0.7	S0?:pec,HII
Mrk 1027	02 11 28.6	04 56 25	9061	123.0	0.9	GGroup
NGC 891	02 19 24.6	42 07 19	529	10.0	13.5	24	88	SA(s)b?:sp,HII
NGC 1022	02 36 04.0	−06 53 35	1503	21.1	2.4	76	34	(R')SB(s)a,HII,Sbrst
NGC 1055	02 39 10.7	00 13 45	996	14.8	7.6	106	69	SBb:sp
NGC 1068	02 40 06.5	−00 13 32	1153	16.7	7.1	90	43	(R)SA(rs)b,Sy2
NGC 1144	02 52 38.4	−00 23 09	8750	118.0	1.1	Ring,Sy2,GPair
NGC 1365	03 31 41.0	−36 18 24	1652	20.8	11.2	32	56	(R')SBb(s)b,Sy1.8
IC 342	03 41 57.2	67 56 30	31	3.7	21.4	0	25	SAB(rs)cd,HII
NGC 1614	04 31 35.7	−08 40 57	4847	63.3	1.3	SB(s)c:pec,HII,Sy2
*VII Zw 31	05 08 15.3	79 36 46	16290	223.4	HII
*IRAS 05189−2524	05 18 58.9	−25 24 40	12810	167.5	pec,Sy2
NGC 2146	06 10 40.1	78 22 23	918	15.2	6.0	123	34	SB(s)ab:pec,HII
NGC 2276	07 10 22.0	85 50 58	2430	35.5	2.8	20	27	SAB(rs)c
Arp 55	09 12 38.1	44 32 26	11957	162.7	0.7	GPair,HII
NGC 2903	09 29 19.9	21 43 19	556	6.2	12.6	17	65	SB(s)d,HII
*UGC 05101	09 32 04.8	61 34 37	11810	160.2	1.1	S?LINER,Sy1.5
M82	09 51 42.9	69 54 59	203	3.5	11.2	65	66	I0,Sbrst,HII
NGC 3079	09 58 35.0	55 55 17	1150	16.2	7.9	165	80	SB(s)c,LINER,Sy2
*IRAS 10565+2448	10 56 36.2	24 48 40	12923	173.3	0.4	LINER,HII

TABLE 1. (continued)

Galaxies ^a	R.A. (1950)	DEC.	$V(\text{km s}^{-1})^b$	$d(\text{Mpc})^c$	$D_{25} (')$	P.A. ^d	Inclination	Classifications ^e
Arp 148	11 01 05.5	41 07 10	10394	143.3	0.6	Ring,GPair
NGC 3556	11 08 36.8	55 56 33	695	10.6	8.8	80	76	SB(s)cd
NGC 3627	11 17 37.9	13 16 08	698	7.6	9.1	173	63	SAB(s)b,Sy2
NGC 3628	11 17 39.6	13 51 48	847	9.6	14.8	104	78	Sb:pec:sp
NGC 3893	11 46 01.1	48 59 20	968	13.9	4.5	165	55	SAB(rs)c
NGC 4030	11 57 50.3	-00 49 22	1460	17.1	4.2	30	45	SA(s)bc
NGC 4041	11 59 39.0	62 24 56	1234	18.0	2.7	...	21	SA(rs)bc
NGC 4414	12 23 57.9	31 30 00	720	9.3	3.6	155	56	SA(rs)c?
NGC 4631	12 39 41.5	32 48 54	620	8.1	15.5	86	80	SB(s)d
NGC 4826	12 54 16.9	21 57 18	408	4.7	10.0	115	57	(R)SA(rs)ab,Sy2
NGC 5005	13 08 38.7	37 19 23	950	14.0	5.8	65	61	SAB(rs)bc,Sy2
NGC 5055	13 13 36.4	42 17 34	504	7.3	12.6	105	55	SA(rs)bc,HII,LINER
NGC 5135	13 22 56.5	-29 34 26	4114	51.7	2.6	...	45	SB(l)ab,Sy2
M83	13 34 11.0	-29 36 48	518	3.7	12.9	45	27	SAB(s)c,HII,Sbrst
*Mrk 273	13 42 51.7	56 08 14	11324	152.4	1.1	Sy2,LINER
NGC 5678	14 30 37.1	58 08 35	1922	27.8	3.3	5	61	SAB(rs)b
NGC 5713	14 37 37.5	-00 04 35	2180	24.0	2.8	10	27	SAB(rs)bc:pec
NGC 5775	14 51 26.8	03 44 53	1690	21.3	4.2	146	78	SBc?:sp
*IRAS 17208-0014	17 20 47.8	-00 14 15	12835	168.0	HII,Sbrst
IRAS 18293-3413	18 29 21.4	-34 13 42	5449	72.1	HII
NGC 6701	18 42 35.5	60 36 08	3950	56.8	1.5	19	...	(R')SB(s)a,HII
NGC 6921 ^f	20 26 20.8	25 33 23	4399	75.5	0.9	141	74	SA(r)0/a

TABLE 1. (continued)

Galaxies ^a	R.A. (1950)	DEC.	$V(\text{km s}^{-1})^b$	$d(\text{Mpc})^c$	$D_{25} (')$	P.A. ^d	Inclination	Classifications ^e
NGC 6946	20 33 49.5	59 58 47	48	5.5	11.5	19	30	SAB(rs)cd,HII
NGC 7130	21 45 19.9	−35 11 01	4842	65.0	1.5	Sa:pec,Sy2,LINER
IC 5179	22 13 13.0	−37 05 30	3447	46.2	2.3	57	61	SA(rs)bc,HII
NGC 7331	22 34 46.7	34 09 21	821	15.0	10.5	90	69	SA(s)b,LINER
NGC 7469	23 00 44.4	08 36 16	4812	67.5	1.5	125	46	(R')SAB(rs)a,Sy1.2
NGC 7479	23 02 26.8	12 03 06	2385	35.2	4.1	25	39	SB(s)c,LINER,Sy2
*IRAS 23365+3604	23 36 32.3	36 04 33	19330	266.1	0.5	Liner
Mrk 331	23 48 53.5	20 18 27	5363	75.3	0.7	S?,HII,Sy2

Notes to Table 1.

Galaxy names marked with * indicates ULIGs with $L_{\text{IR}} \gtrsim 10^{12} L_{\odot}$. Galaxies with HCN data available in the literature that have been included in our HCN sample are not listed (see Table 1 in the companion paper [Gao & Solomon 2003, Paper II] for these galaxies).

^aGalaxies that were mapped along the major axes are marked in boldface and the details will be discussed in a future paper (Gao & Solomon in preparation).

^bHeliocentric velocity drawn from the literature and NED or determined from our CO observations.

^cSource distance is calculated using $H_0 = 75 \text{ km s}^{-1} \text{ Mpc}^{-1}$ corrected for the local group motion, except for a few nearby galaxies, where the most recent and commonly used values in the literature are adopted.

^dPosition angles of the major axes, except for NGC 1068 and IC 342, that are used in mapping HCN emission.

^eAlmost entirely from NED, GPair=galaxy pair, GGroup=galaxy group, Sbrst=starburst galaxy, Ring=ring galaxy.

^fNGC 6921 is most likely only partially associated with the *IRAS* source IRAS 20264+2533, which is possibly more related to the galaxy MCG +04-48-002, $\sim 1'.5$ east of NGC 6921 (Sanders et al. 2003). NGC 6921 was included in our HCN survey since Young et al. (1986) reported relatively strong CO emission and assumed that the *IRAS* emission comes entirely from NGC 6921.

Table 2. Telescope Efficiencies at 3 mm^a

Telescope	Typical T_{sys}	T Scale	η_{M}^* ^b	F_{eff}^c	B_{eff}^c	η_{B}^d
NRAO 12m	220 (250)K	T_{R}^*	0.89 (0.83)			
IRAM 30m	250 (270)K	T_{A}^*		0.92 (0.92)	0.75 (0.65)	
FCRAO 14m	500 (850)K	T_{A}^*				0.60 (0.55)

^aBoth values at 3.4 mm for HCN J=1-0 and at 2.6 mm for CO J=1-0 (in parentheses) are given. These efficiencies were adopted for conversion from the measured antenna temperature scale to the main-beam T_{mb} scale.

^b $T_{\text{mb}} = T_{\text{R}}^*/\eta_{\text{M}}^*$, where η_{M}^* is the corrected main-beam efficiency.

^c $T_{\text{mb}} = T_{\text{A}}^*(F_{\text{eff}}/B_{\text{eff}})$, where F_{eff} and B_{eff} are the forward and effective beam efficiencies respectively.

^d $T_{\text{mb}} = T_{\text{A}}^*/\eta_{\text{B}}$, where $\eta_{\text{B}} = B_{\text{eff}}/F_{\text{eff}}$ is the main-beam efficiency.

TABLE 4. Observed Quantities in the HCN Survey

Galaxies	Offsets "	I_{HCN}	σ_{HCN} K km s ⁻¹	I_{CO}	σ_{CO}	V_{CO} km s ⁻¹	ΔV	$\frac{f_{60\mu\text{m}}}{f_{100\mu\text{m}}}$	$f_{100\mu\text{m}}$ Jy	$\frac{\int I_{\text{HCN}} d\Omega_s}{\Omega_{\text{mb}}}$ K km s ⁻¹	$\frac{\int I_{\text{CO}} d\Omega_s}{\Omega_{\text{mb}}}$	$S_{\text{CO}} \Delta V$ Jy km s ⁻¹	$S_{\text{HCN}} \Delta V$
NGC 253	map ^{a,b}	23.0	0.6	272.0	1.6	251.9	202.4	0.54	1857.8	33.5	850.5	24523.0	947.5
	map ^{a,c}	74.2	1.5					153.8	770.5
IC 1623 ^b	0, 0	.81	.15	20.6	0.4	6076	103	0.77	30.6	.91	24.8	745.0	27.3
NGC 660 ^b	0, 0	.85	.20	31.7	1.6	825	316	0.63	103.8	>0.96	45.0	>1145.8	>28.0
NGC 695 ^c	0, 0	1.4	.24	9727	165	0.55	14.2	1.4	7.3 ^d	214.5	6.7
Mrk 1027 ^c	0, 0	0.91	.17	29.1	.90	9007	150	0.64	8.5	.91	29.1	136.0	4.4
NGC 891	map ^{a,e}	0.85	0.42	35.5	2.1	548	160	0.31	198.6	<2.71	158.8	3733.7	<63.6
	map ^{a,c}	4.8	0.5					14.5	71.5
NGC 1022 ^b	0, 0	.28	.09	9.6	.37	1463	89	0.75	26.8	0.32	11.6	337.7	9.4
NGC 1055 ^b	0, 0	<.96	.48	0.36	63.8	<1.1	75.3 ^d	2221.4	<31.3
NGC 1068	map ^{a,e}	6.6	0.6	69.0	2.8	1185	175	0.79	251.8	13.0	155.7	3651.1	302.2
NGC 1144 ^c	0, 0	.82	0.24	46.2	1.0	8750	650	0.46	11.6	0.82	46.2	216.9	3.5
NGC 1365	map ^{a,b}	2.2	0.3	55.7	1.6	1623.4	233.4	0.45	185.4	5.5	168.0	3710.0	179.8
IC 342	map ^{a,b}	3.4	0.3	50.0	0.8	35.2	72.8	0.39	660.7	18.0	808.2	18962.0	522.0
	map ^{a,e}	3.2	0.3	49.7	0.8	32.0	70.0						
NGC 1614 ^c	0, 0	1.5	.22	43.5	1.2	4750	184	0.96	33.0	1.5	43.5	208.8	7.2
VII Zw 31 ^c	0, 0	1.1	.17	21.0	0.9	16275	200	0.55	9.8	1.1	21.0	99.0	5.3
IRAS 05189–2524 ^c	0, 0	1.1	.20	12831	110	1.1	12.0	1.1	3.1 ^d	92.4	5.3
NGC 2146	map ^{a,e}	1.9	0.3	50.1	1.8	891	311	0.71	204.2	<4.5	105.7	2491.2	<106.2
	map ^{a,c}	8.1	0.6							21.2	413.2	2400.0	104.1
NGC 2276 ^b	0, 0	.23	.06	8.3	.19	2405	61	0.42	30.8	0.25	10.1	292.6	6.8
Arp 55 ^c	0, 0	.81	.15	11945	165	0.59	10.1	0.81	6.1 ^d	181.3	3.8
NGC 2903 ^b	0, 0	1.7	0.25	27.8	0.8	564.5	155.6	0.36	147.2	>1.7	~ 72.0	2105.0	48.6
	map ^{a,c}	4.4	0.5					~ 10.0	~ 414.0 ^d	1987.2	48.0
UGC 5101 ^c	0, 0	2.1	.33	15.6	0.7	11785	245	0.59	20.4	2.1	15.6	73.3	10.4
M82	map ^{a,b}	6.6	0.4	192.7	2.1	235.5	180.5	0.94	1349.0	15.6	607.7	17671.9	458.7
	map ^{a,c}	27.4	1.4					93.0	445.2
	map ^{a,e}	8.2	0.7	257.6	1.9	198.5				22.0	660.0	15648.5	507.2

TABLE 4. (continued)

Galaxies	Offsets "	I_{HCN}	σ_{HCN} K km s ⁻¹	I_{CO}	σ_{CO}	V_{CO} km s ⁻¹	ΔV	$\frac{f_{60\mu\text{m}}}{f_{100\mu\text{m}}}$	$f_{100\mu\text{m}}$ Jy	$\frac{\int I_{\text{HCN}} d\Omega_s}{\Omega_{\text{mb}}}$ K km s ⁻¹	$\frac{\int I_{\text{CO}} d\Omega_s}{\Omega_{\text{mb}}}$	$S_{\text{CO}} \Delta V$ Jy km s ⁻¹	$S_{\text{HCN}} \Delta V$
NGC 3079 ^b	0, 0	2.6	.42	66.1	1.1	1111	365	0.48	103.5	2.9	110.0	3187.5	77.6
IRAS 10565+2448 ^c	0, 0	1.8	.20	16.5	0.6	12950	380	0.85	14.4	1.8	16.5	77.5	8.6
Arp 148 ^c	0, 0	1.1	.16	10520	220	0.57	10.7	1.1	18.3 ^d	86.0	5.4
NGC 3556 ^b	0, 0	.50	.08	10.1	.80	674	89	0.40	80.7	.57	40.0	1032.5	16.8
NGC 3627 ^b	0, 0	.68	.12	687	159	0.39	144.9	>0.76	190.7 ^d	4477.4	>21.4
NGC 3628	map ^{a,b}	1.2	0.2	57.8	1.1	844.1	193.7	0.40	121.9	3.1	185.5	4351.8	90.2
NGC 3893 ^b	0, 0	.80	.13	8.9	.34	968	152	.39	38.2	0.90	26.6	626.5	26.0
NGC 4030 ^b	0, 0	1.2	.26	20.4	.68	1458	232	0.38	50.4	1.35	65.1	1879.9	39.3
NGC 4041 ^b	0, 0	.35	.07	12.2	.48	1212	116	0.43	32.6	0.40	15.0	433.6	11.7
NGC 3079 ^b	0, 0	2.6	.42	66.1	1.1	1111	365	0.48	103.5	2.9	110.0	3187.5	77.6
NGC 4414 ^b	0, 0	1.2	0.3	30.4	.70	706	269	0.38	68.4	~1.0	66.3	1982.0	38.5
NGC 4631 ^b	0, 0	.72	.16	12.1	.95	658	75	0.40	208.4	>0.92	40.5	1167.0	>27.1
	map ^{a,e}	1.1	0.3	18.5	1.2	603	125			2.1	49.6	1166.0	49.3
NGC 4826 ^b	0, 0	1.0	.17	22.2	1.6	372	216	0.49	75.7	>1.4	75.0	2172.6	>40.1
NGC 5005 ^b	0, 0	1.3	.25	18.7	1.5	1034	210	0.32	59.4	2.6	87.7	2542.3	75.4
	45, 21	0.75	.25	10.0	1.5	1176	60						
NGC 5055 ^b	0, 0	1.5	.15	18.8	1.3	500	226	0.25	157.4	>1.6	200.1	4690.5	>46.5
NGC 5135 ^b	0, 0	.70	.08	11.0	.45	4111	92	0.58	29.0	0.74	14.5	426.3	21.2
M83	map ^{a,b}	63.7	5.4	2.5	0.3	508.5	75.1	0.42	638.3	12.9	557.1	13085.2	376.6
Mrk 273 ^c	0, 0	3.5	.47	22.7	.89	11320	357	1.1	22.3	3.5	22.7	107.0	16.8
NGC 5678 ^b	0, 0	.71	.22	10.8	1.0	1928	266	0.36	26.7	.81	28.0	811.7	23.1
NGC 5713 ^b	0, 0	.25	.07	14.4	.30	1913	97	0.28	37.2	0.48	17.5	505.9	10.0
NGC 5775 ^b	0, 0	.80	.25	12.5	1.4	1697	151	0.46	51.4	~0.90	35.6	868.7	26.5

TABLE 4. (continued)

Galaxies	Offsets "	I_{HCN}	σ_{HCN}	I_{CO}	σ_{CO}	V_{CO}	ΔV	$\frac{f_{60\mu\text{m}}}{f_{100\mu\text{m}}}$	$f_{100\mu\text{m}}$	$\frac{\int I_{\text{HCN}} d\Omega_s}{\Omega_{\text{mb}}}$	$\frac{\int I_{\text{CO}} d\Omega_s}{\Omega_{\text{mb}}}$	$S_{\text{CO}}\Delta V$	$S_{\text{HCN}}\Delta V$
			K km s ⁻¹			km s ⁻¹			Jy	K km s ⁻¹		Jy km s ⁻¹	
IRAS 17208–0014 ^b	0, 0	.91	.19	5.7	0.3	12855	303	0.98	34.9	1.0	6.9	206.5	30.5
IRAS 18293–3413 ^b	0, 0	.50	.16	16.8	1.0	5490	210	0.69	53.8	0.56	20.4	591.8	16.1
NGC 6701 ^b	0, 0	.28	.06	10.8	.20	3946	88	0.48	21.4	0.31	13.1	380.9	9.0
NGC 6921 ^b	0, 0	.50	0.1	5.0 ^d	.31	4200	397	0.54	18.5	0.56	6.0	182.0	16.5
NGC 6946	map ^{a,b}	2.6	0.2	58.5	1.4	37.7	125.0	0.40	344.4	11.5	380.0	11400.5	327.8
	map ^{a,c}	11.4	1.0					59.5	292.6
NGC 7130 ^b	0, 0	.50	.11	10.9	.90	4842	87	0.64	26.6	0.57	13.2	383.0	16.5
IC 5179 ^b	0, 0	1.1	.20	12.7	1.6	3418	242	0.50	38.5	1.2	15.4	446.6	37.1
NGC 7331 ^b	0, 0	1.3	.27	16.0	1.1	871	198	0.31	114.8	>1.5	>59.4	>1752.3	<42.8
NGC 7469 ^b	0, 0	.31	.06	8.3	.60	4925	177	0.78	35.4	0.35	10.1	293.8	10.5
NGC 7479 ^b	0, 0	.60	.12	11.0	.54	2368	192	0.59	26.2	0.67	26.7	787.6	20.2
IRAS 23365+3604 ^c	0, 0	1.2	.24	10.9	0.5	19300	68	0.94	8.2	1.2	10.9	51.2	5.9
Mrk 331 ^b	0, 0	.38	.11	8.6	.65	5410	215	0.81	21.0	0.43	11.4	336.3	12.9

Notes to Table 4.

The parameters/quantities listed are: galaxy name (column 1); observed position (off-sets or major-axis mapping) as given in Table 1 (column 2); measured line intensities and estimated errors for HCN and CO respectively in columns 3 to 6, but CO data taken from literature are not listed; heliocentric velocity of the galaxy as determined from either our CO observations or CO data in literature and the linewidth (FWHM) in column 7, 8; the *IRAS* far-IR flux density ratio $f_{60\mu\text{m}}/f_{100\mu\text{m}}$ and 100 μm flux (column 9, 10); the integrated line intensities over the entire source on the main-beam antenna temperature scale for HCN and CO (column 11, 12); and the total CO and HCN line emission fluxes (last two columns).

^aMultiple position HCN and CO observations along the major axes are available (Gao & Solomon in preparation). Here only the central position (0, 0) data are given.

^bData from the NRAO 12m are on the temperature scale of T_{R}^* . Only NGC 1055 was not detected and is listed as a 2σ upper limit. However, there are still limits in the total integrated HCN fluxes in some nearby galaxies because of either only one measurement towards the center (lower limits) or non-detections at large galactic radii but detected at the centers/inner disks (upper limits).

^cData from the IRAM 30m are converted to the main beam temperature scale.

^dCO data from literature: NGC 695, IRAS05189-2524, Arp 55 from Sanders et al. (1991); Arp 148 from Horellou et al. (1995); NGC 1055 from Sage (1987); NGC 1365 from Sandqvist, Jörsäter, & Lindblad (1995); NGC 2903 from Jackson et al. (1991); NGC 6921 from this work, but Young et al. (1986, 1995) listed the line intensity twice as large as ours (see more notes for NGC 6921 in Table 1).

^eData from the FCRAO 14m are expressed on the main beam temperature scale. In most cases, only the central beams covering the nuclear regions have HCN detections. The total integrated HCN line fluxes have been derived using the weak detections or the 2σ upper limits from other beams covered by QUARRY along the major axes along with the central beam measurements.

Table 4. Global Properties of Galaxies in the HCN Survey

Galaxies	L_{IR} $10^{10} L_{\odot}$	L_{CO} $10^8 \text{ K km s}^{-1} \text{ pc}^2$	$L_{\text{HCN}}^{\text{a}}$	$L_{\text{HCN}}/L_{\text{CO}}$	$\frac{L_{\text{IR}}}{M_{\text{dense}}(\text{H}_2)}^{\text{b}}$ L_{\odot}/M_{\odot}	$\frac{L_{\text{IR}}}{M(\text{H}_2)}$
NGC 253	2.1	4.6	0.27	0.059	77.8	9.6
IC 1623	46.7	130.5	8.5	0.065	55.0	7.5
NGC 660	3.7	7.3	>0.26	>0.036	<142.3	10.6
NGC 695	46.6	92.9	4.3	0.046	108.4	10.5
MRK 1027	25.7	41.7	1.89	0.045	136.0	12.9
NGC 891	2.6	11.0	0.25	0.024	104.0	5.4
NGC 1022	2.6	4.2	0.20	0.047	131.5	13.1
NGC 1055	2.1	13.3	<0.37	<0.028	>56.9	3.3
NGC 1068	28.3	20.7	3.61	0.174	78.5	28.6
NGC 1144	25.1	108.9	2.67	0.025	94.0	4.8
NGC 1365	12.9	58.7	3.10	0.053	41.6	4.6
IC 342	1.4	9.4	0.47	0.050	30.2	3.4
NGC 1614	38.6	24.5	1.25	0.051	306.8	33.2
*VIIZw31	87.1	125.0	9.8	0.078	88.9	14.6
*05189–2524	118.1	67.0	6.2	0.093	190.4	36.9
NGC 2146	10.0	12.5	0.96	0.071	122.4	16.8
NGC 2276	6.2	10.2	0.40	0.039	156.0	12.8
ARP 55	45.7	125.0	3.8	0.030	120.2	7.6
NGC 2903	0.83	2.3	>0.09	>0.036	<104.0	7.6
*UGC 05101	89.2	50.8	10.0	0.197	89.2	36.7
M82	4.6	5.7	0.30	0.053	153.3	16.9
NGC 3079	4.3	24.0	~1.0	~0.042	~43.5	3.7
*10566+2448	93.8	61.5	10.2	0.166	92.0	32.0
ARP 148	36.5	>47.0	4.0	<0.085	91.2	<16.2
NGC 3556	1.35	>4.5	>0.09	~0.020	<155.0	<6.3
NGC 3627	1.26	4.4	>0.08	>0.017	<160.0	6.0
NGC 3628	1.01	7.1	0.24	0.034	43.5	3.3
NGC 3893	1.15	4.1	0.23	0.056	50.4	5.9
NGC 4030	2.14	15.2	0.54	0.036	40.0	3.0
NGC 4041	1.70	3.9	0.18	0.046	94.8	9.1
NGC 4414	0.81	4.6	0.16	0.033	54.8	3.7
NGC 4631	2.0	2.3	~0.09	~0.039	~222.2	18.5
NGC 4826	0.26	1.3	>0.04	>0.030	<65.5	4.1
NGC 5005	1.4	8.2	0.41	0.049	21.5	2.2

Table 4—Continued

Galaxies	L_{IR} $10^{10} L_{\odot}$	L_{CO} $10^8 \text{ K km s}^{-1} \text{ pc}^2$	$L_{\text{HCN}}^{\text{a}}$ $10^8 \text{ K km s}^{-1} \text{ pc}^2$	$L_{\text{HCN}}/L_{\text{CO}}$	$\frac{L_{\text{IR}}}{M_{\text{dense}}(H_2)}^{\text{b}}$ L_{\odot}/M_{\odot}	$\frac{L_{\text{IR}}}{M(H_2)}$
NGC 5055	1.1	8.6	>0.10	>0.012	<111.0	2.7
NGC 5135	13.8	31.3	2.73	0.087	50.6	9.1
M83	1.4	8.1	0.35	0.043	40.5	3.7
*MRK 273	129.9	65.0	15.2	0.234	85.5	41.8
NGC 5678	3.0	17.2	0.75	0.044	40.0	3.6
NGC 5713	4.2	8.1	0.22	0.027	188.9	10.7
NGC 5775	3.8	10.9	0.57	0.052	66.7	7.2
*17208–0014	234.5	146.9	37.6	0.256	62.4	33.4
18293–3413	53.7	85.5	4.03	0.047	66.6	13.2
NGC 6701	11.2	34.0	1.38	0.041	40.6	6.9
NGC 6921	11.4	17.5	~2.81	~0.160	~41.0	13.6
NGC 6946	1.6	9.2	0.49	0.053	33.5	3.6
NGC 7130	21.4	44.9	3.27	0.071	65.4	10.0
IC 5179	14.1	~26.4	3.42	~0.129	41.2	~11.2
NGC 7331	3.5	>10.7	>0.44	~0.041	<79.8	<6.8
NGC 7469	40.7	37.1	2.19	0.059	185.4	23.0
NGC 7479	7.4	26.7	1.12	0.042	66.1	5.8
*23365+3604	142.0	85.0	15.0	0.176	94.6	35.0
MRK 331	26.9	52.1	3.35	0.064	80.3	10.7

^aThe 2σ upper limit is listed for NGC 1055. The lower limits are for nearby galaxies where we only detected HCN in the galaxy centers or extensive mapping is still required in order to estimate the total HCN and CO luminosities.

^b $M_{\text{dense}} = 10L_{\text{HCN}} M_{\odot}/\text{K km s}^{-1} \text{ pc}^2$ and $M(H_2) = 4.78L_{\text{CO}} M_{\odot}/\text{K km s}^{-1} \text{ pc}^2$, see §4.5.

Note. — ULIGs with $L_{\text{IR}} \gtrsim 10^{12} L_{\odot}$ are indicated by asterisks (*).

Fig. 1.— (a) The distribution of infrared luminosities in our HCN survey sample of 53 galaxies plus a dozen galaxies with published HCN observations. More than half of the sample galaxies have $L_{\text{IR}} < 10^{11}L_{\odot}$ and most of them have $L_{\text{IR}} < 3 \times 10^{10}L_{\odot}$. (b) The distribution of CO luminosities in the same 65 galaxies. (c) The distribution of HCN luminosities in the same sample.

Fig. 2.— The HCN spectra observed with the IRAM 30m telescope. The vertical axis is the main-beam temperature scale in units of mK. For nearby galaxies, only the central spectra are shown here. CO spectra (dashed lines) from the same telescope have been divided by indicated factors for comparison. The spectra are ordered by right ascension, as in Table 1. Some spectra are CO J=2-1, which have a much smaller beam size than the HCN J=1-0 observations. Some frames have only the CO line emission windows (derived from published data) indicated. For NGC 253, we show the CO J=2-1 spectrum obtained from the NRAO 12m (scaled to the main-beam temperature scale for proper comparison), which has roughly the same beam size as that of the HCN J=1-0 from the IRAM 30m.

Fig. 3.— HCN spectra obtained from the NRAO 12m telescope. The temperature scale is T_R^* in mK. $T_{mb} = T_R^*/\eta_M^*$, with a corrected beam efficiency $\eta_M^* \sim 0.89$. As in Fig. 2, only the central spectra are shown here for nearby galaxies and a few of them (NGC 253, NGC 2903, M82, and NGC 6946) are the observations done at both the 12m and 30m telescopes. The dashed lines are CO J=1-0 spectra divided by indicated factors. The ultraluminous infrared galaxy IRAS 17208–0014 (the only one observed with the 12m) is shown last. The spectra of NGC 1068 (obtained from the FCRAO 14m) and NGC 1055 (not detected) are not shown.

Fig. 4.— HCN and IR luminosities in our HCN survey sample (*open circles*) compared with the original correlation proposed by Solomon et al. (1992) for only 10 galaxies (*circles with asterisks*). Note that we used the IR luminosity rather than the far-IR luminosity as in Solomon et al. (1992). Representative error bar is shown for the highest L_{HCN} in the sample, which includes $\sim 20\%$ calibration uncertainty. The line indicates $\log L_{\text{IR}} = 0.97 \log L_{\text{HCN}} + 3.1$ (see text).

Fig. 5.— (a) Relationship between the HCN luminosity and the luminosity ratio of the 12 μm -to-IR emission. (b) The HCN-to-CO luminosity ratio is plotted against the ratio of the 12-to-100 μm emission. There are no significant correlations found implying that galaxies with excess mid-IR emission do not show stronger HCN emission and do not contain higher fractions of dense molecular gas. The sample is divided into luminous and ultraluminous galaxies (LIGs/ULIGs) with $L_{\text{IR}} \geq 10^{11}L_{\odot}$ (*filled circles*) and less luminous galaxies (*open circles*). Representative error bar is also shown for the highest L_{HCN} .

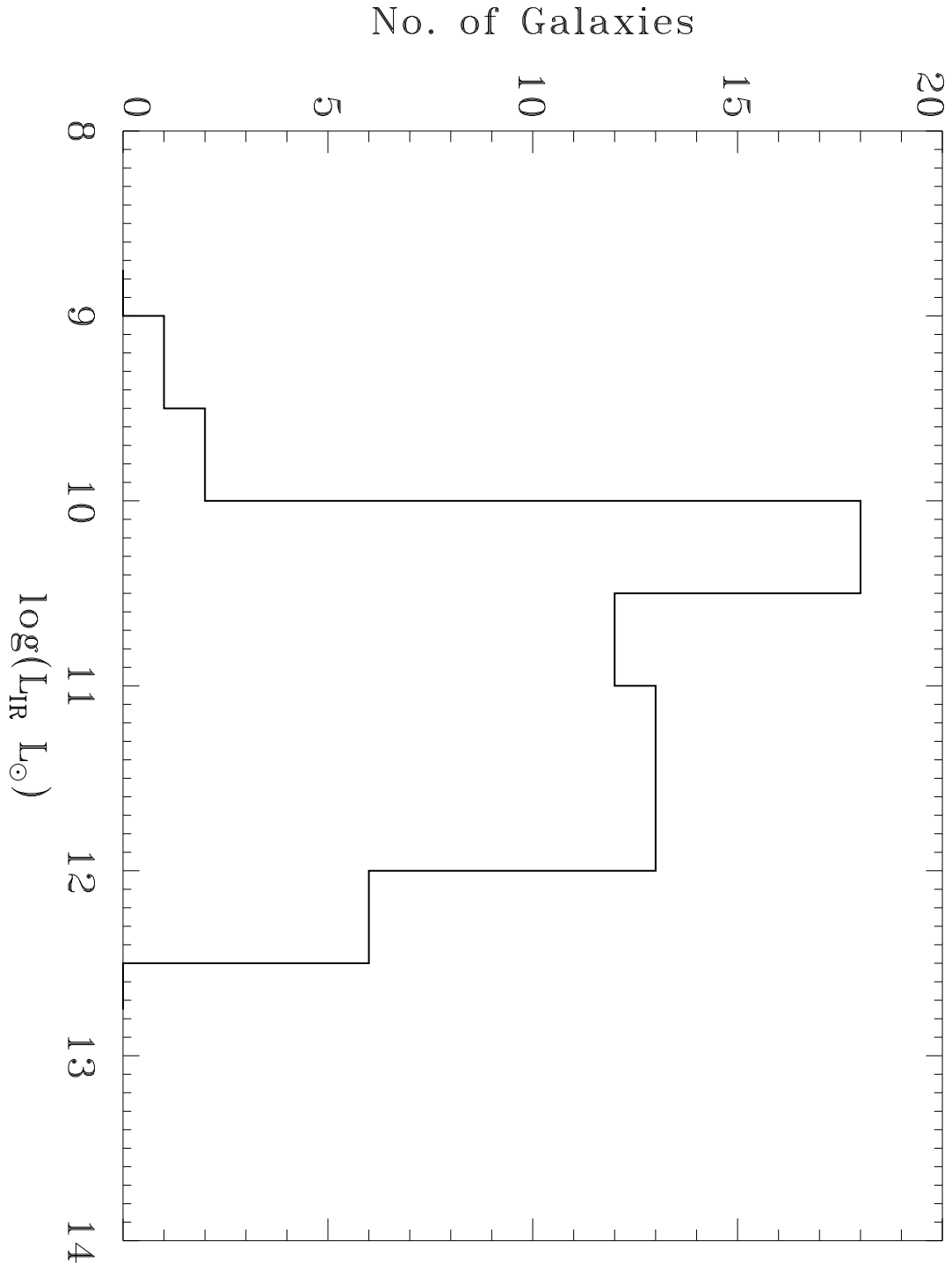


Fig. 1a

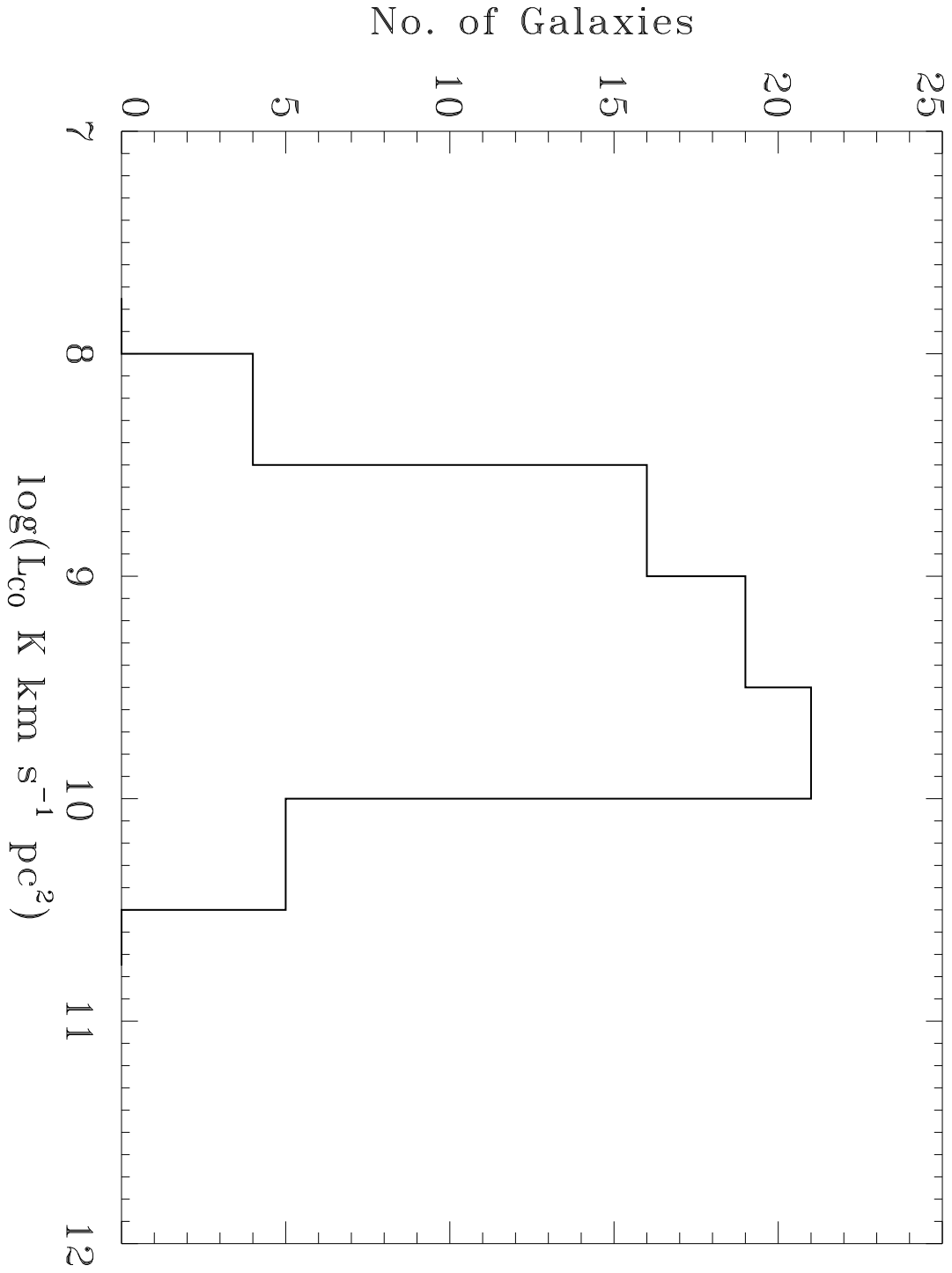


Fig. 1b

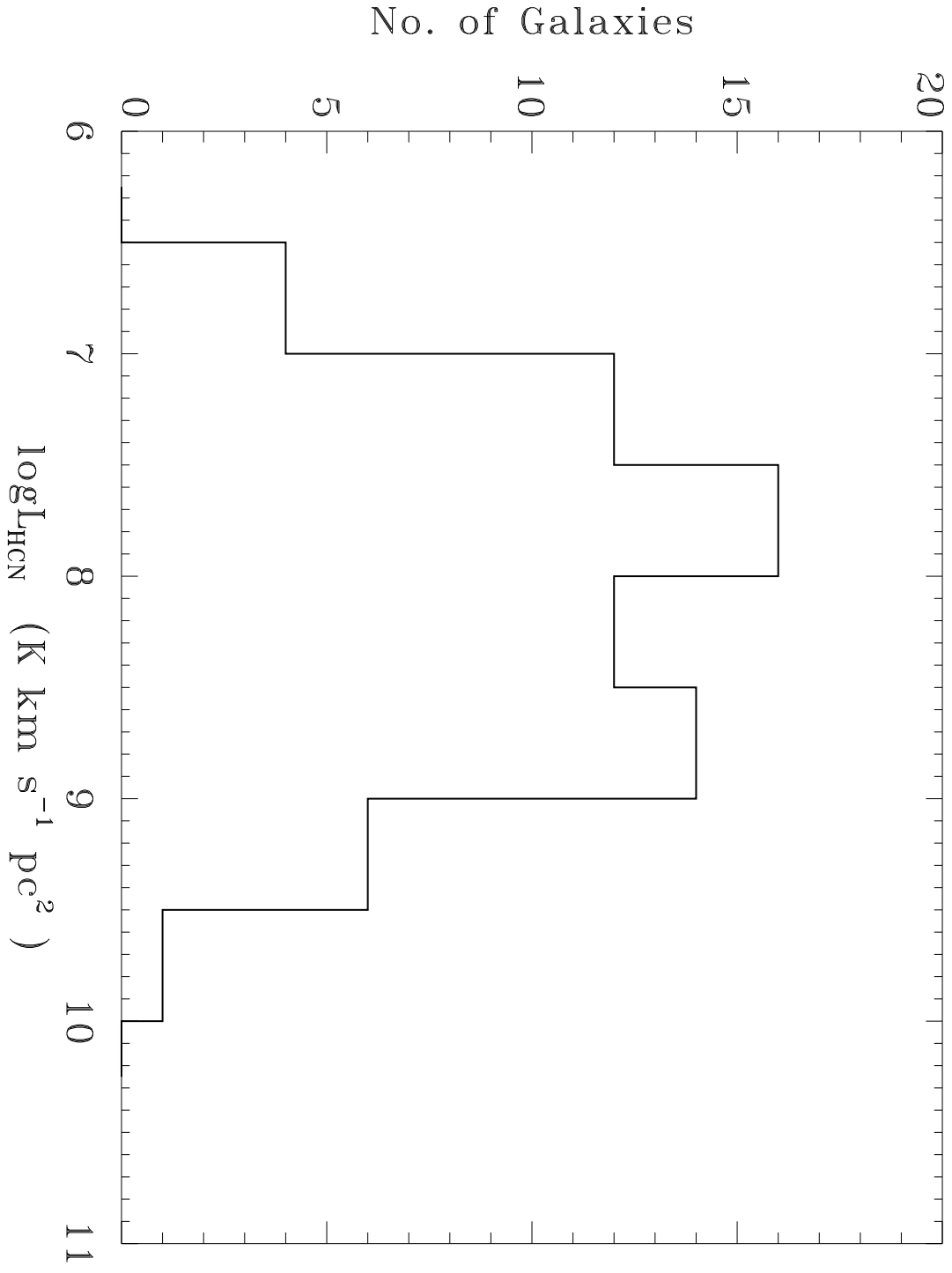


Fig. 1c

Fig. 2a See 0310341.fig2a.gif

Fig. 2b
See 0310341.fig2b.gif

Fig. 2c
See 0310341.fig2c.gif

Fig. 3a
See 0310341.fig3a.gif

Fig. 3b
See 0310341.fig3b.gif

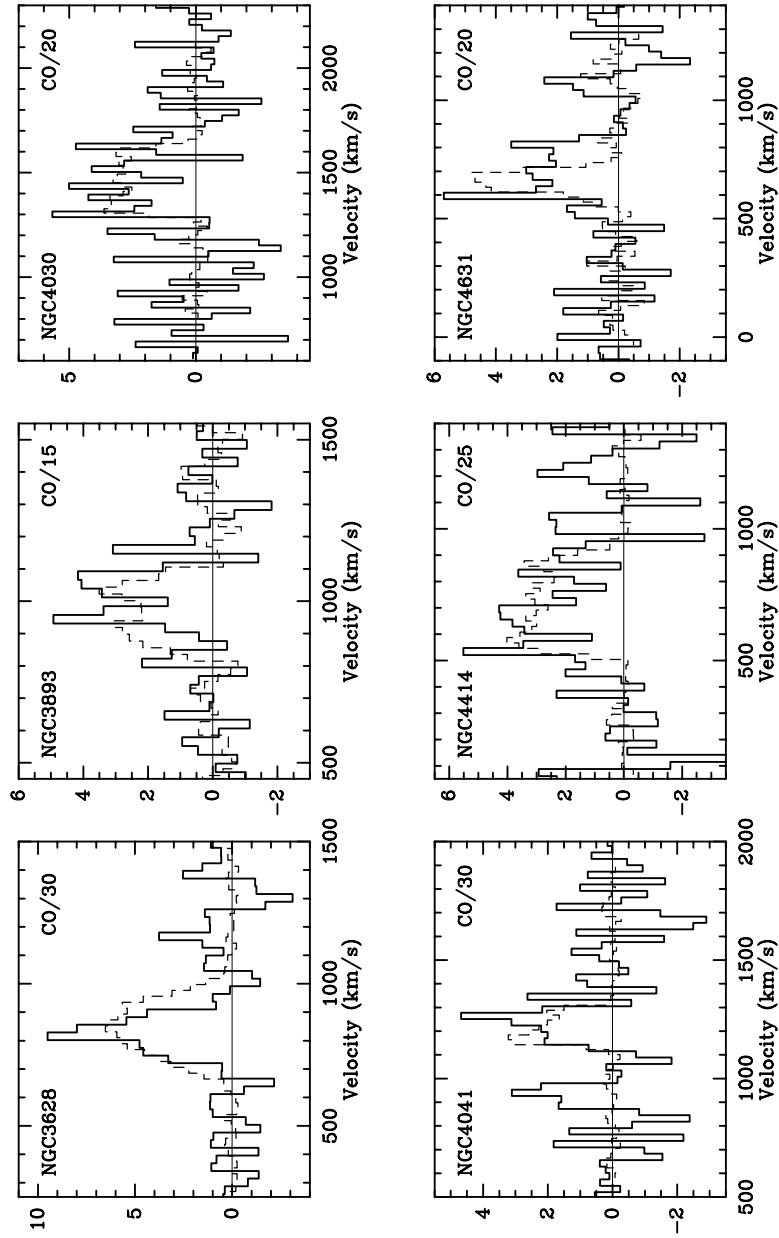


Fig. 3c

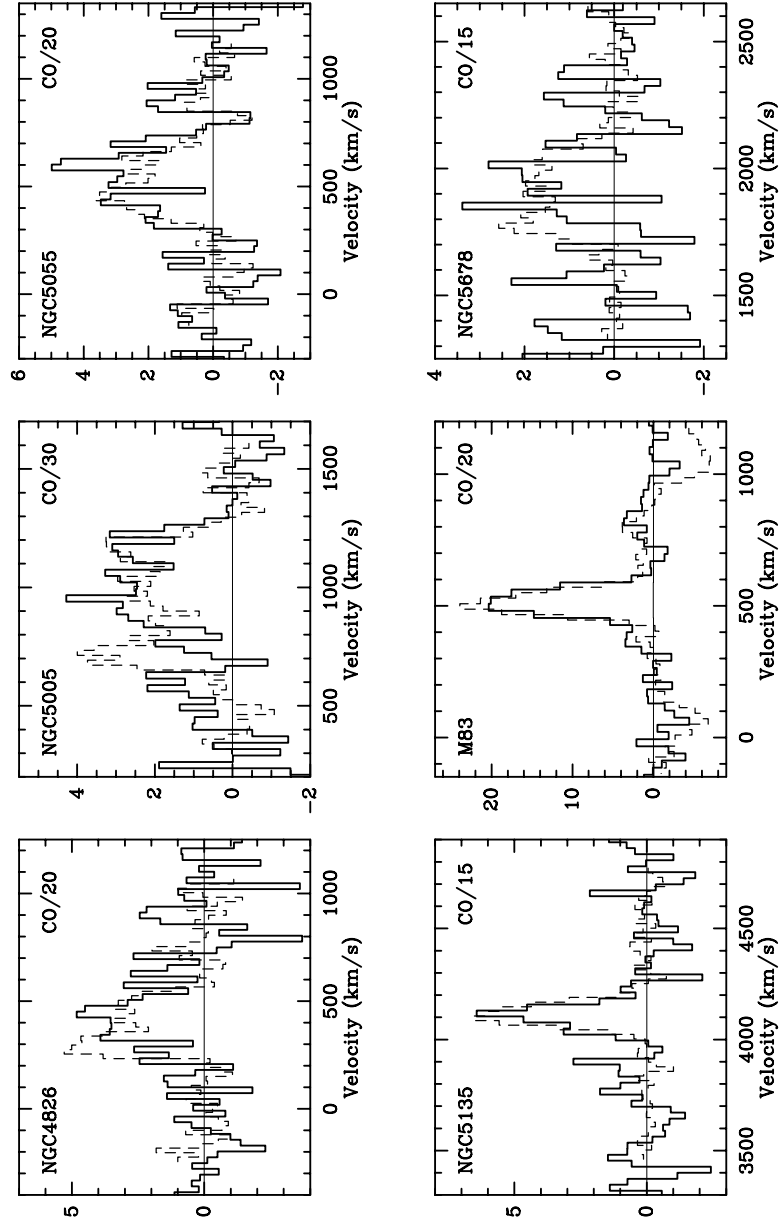


Fig. 3d

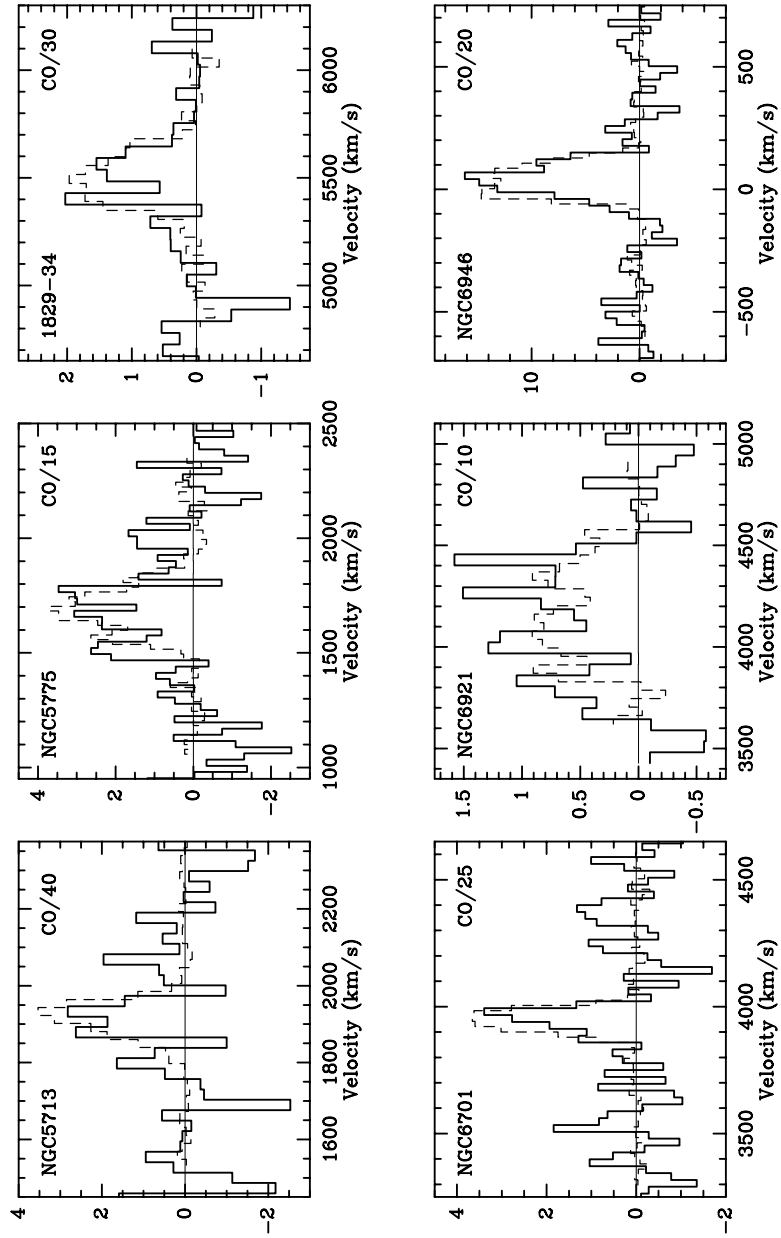


Fig. 3e

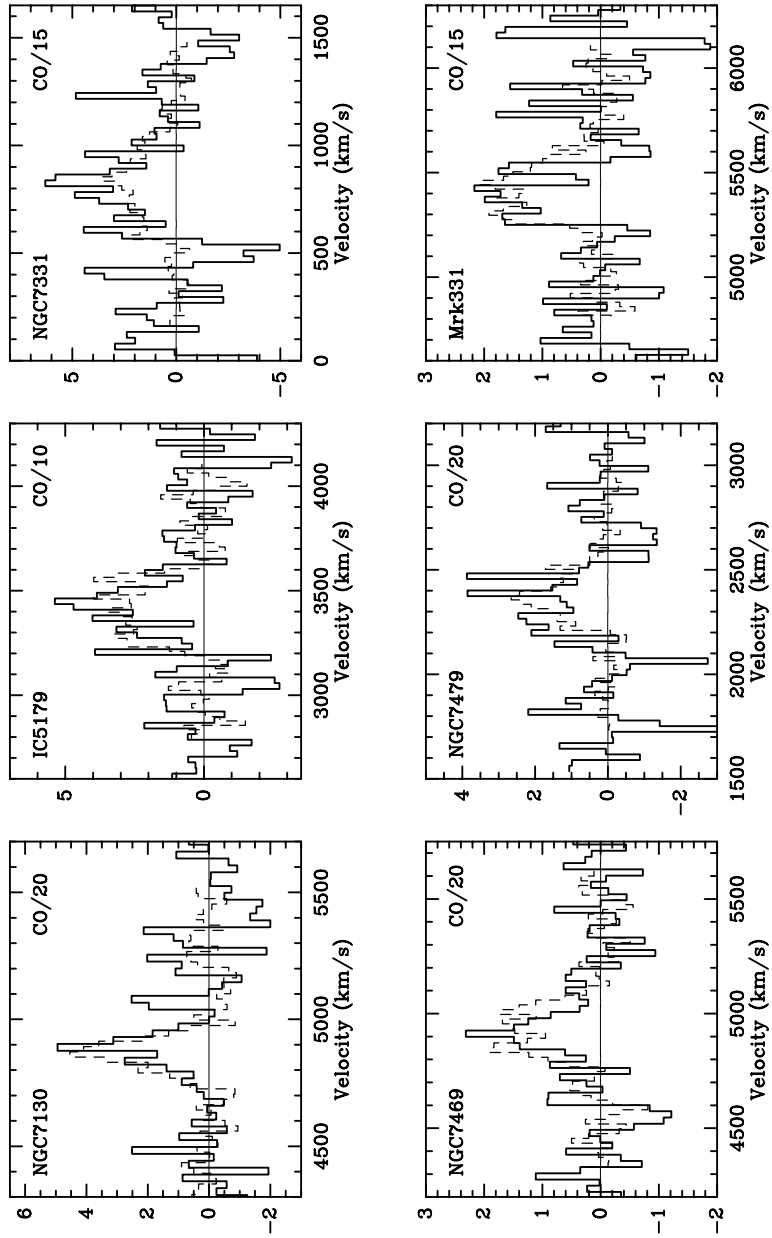


Fig. 3f

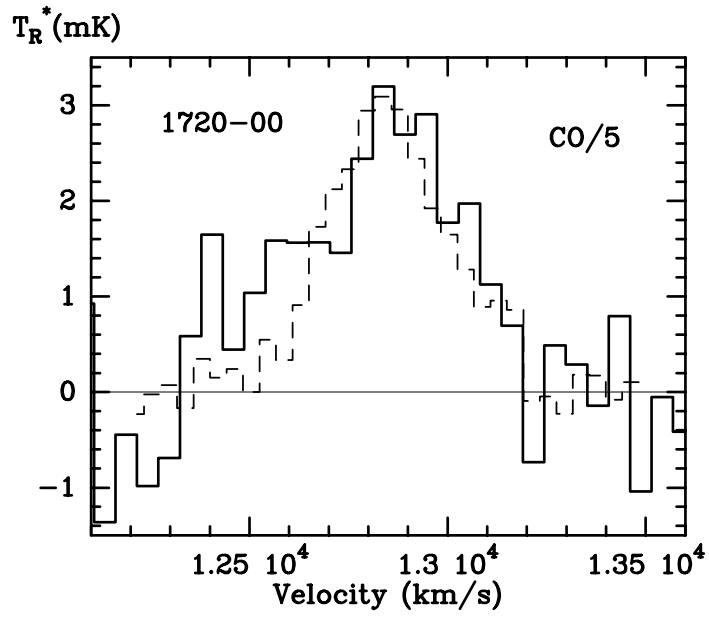


Fig. 3g

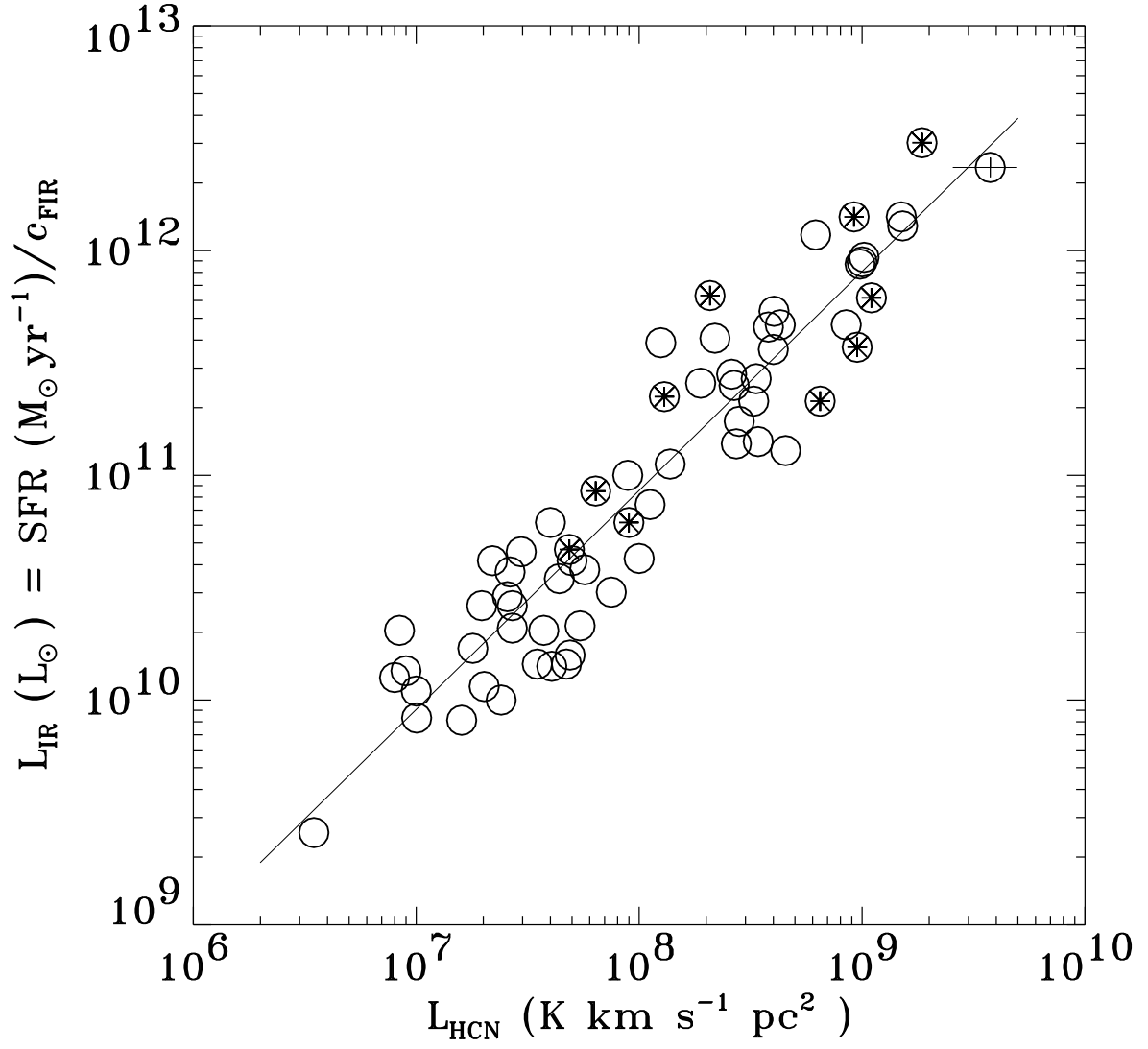


Fig. 4

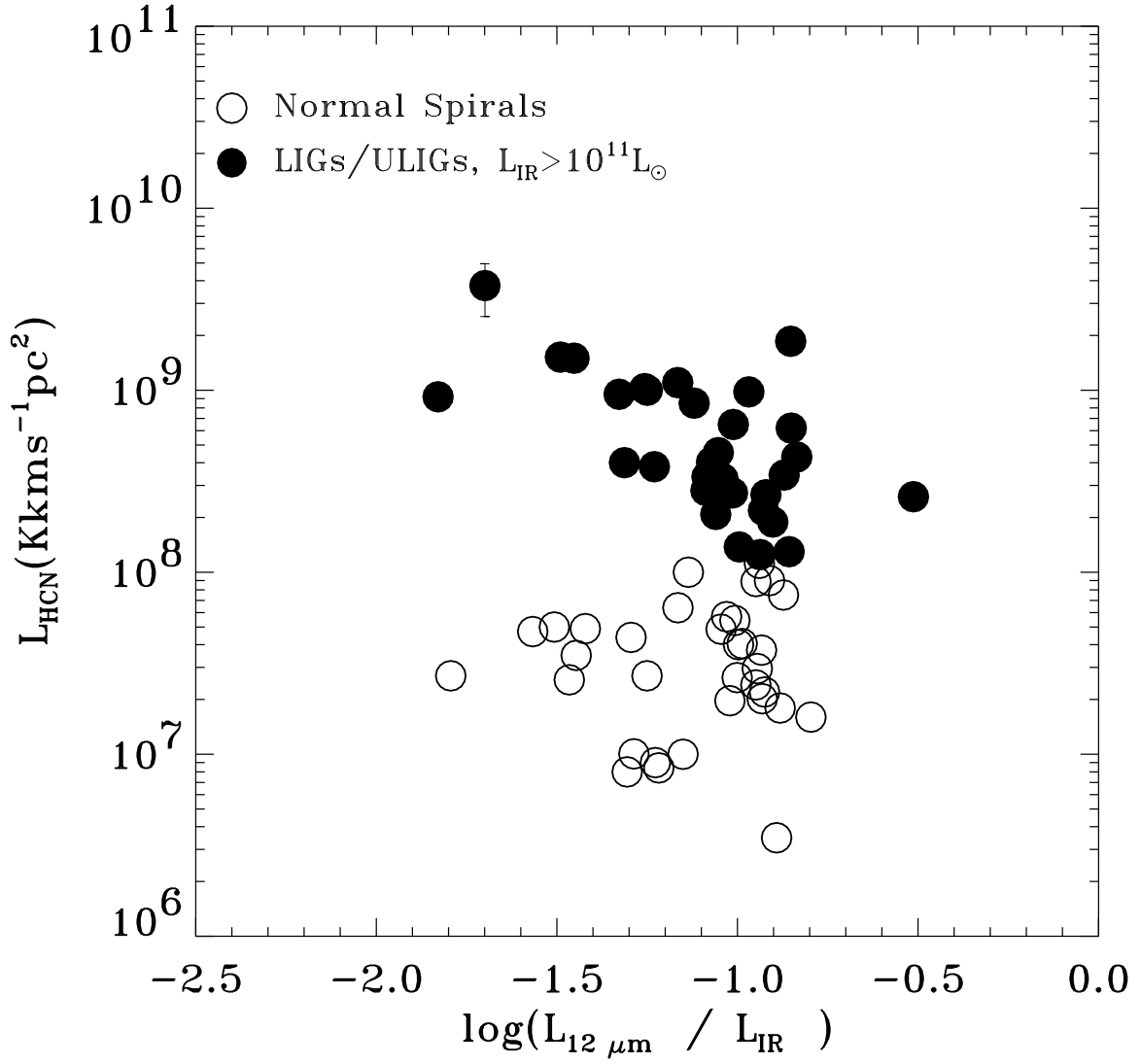


Fig. 5a

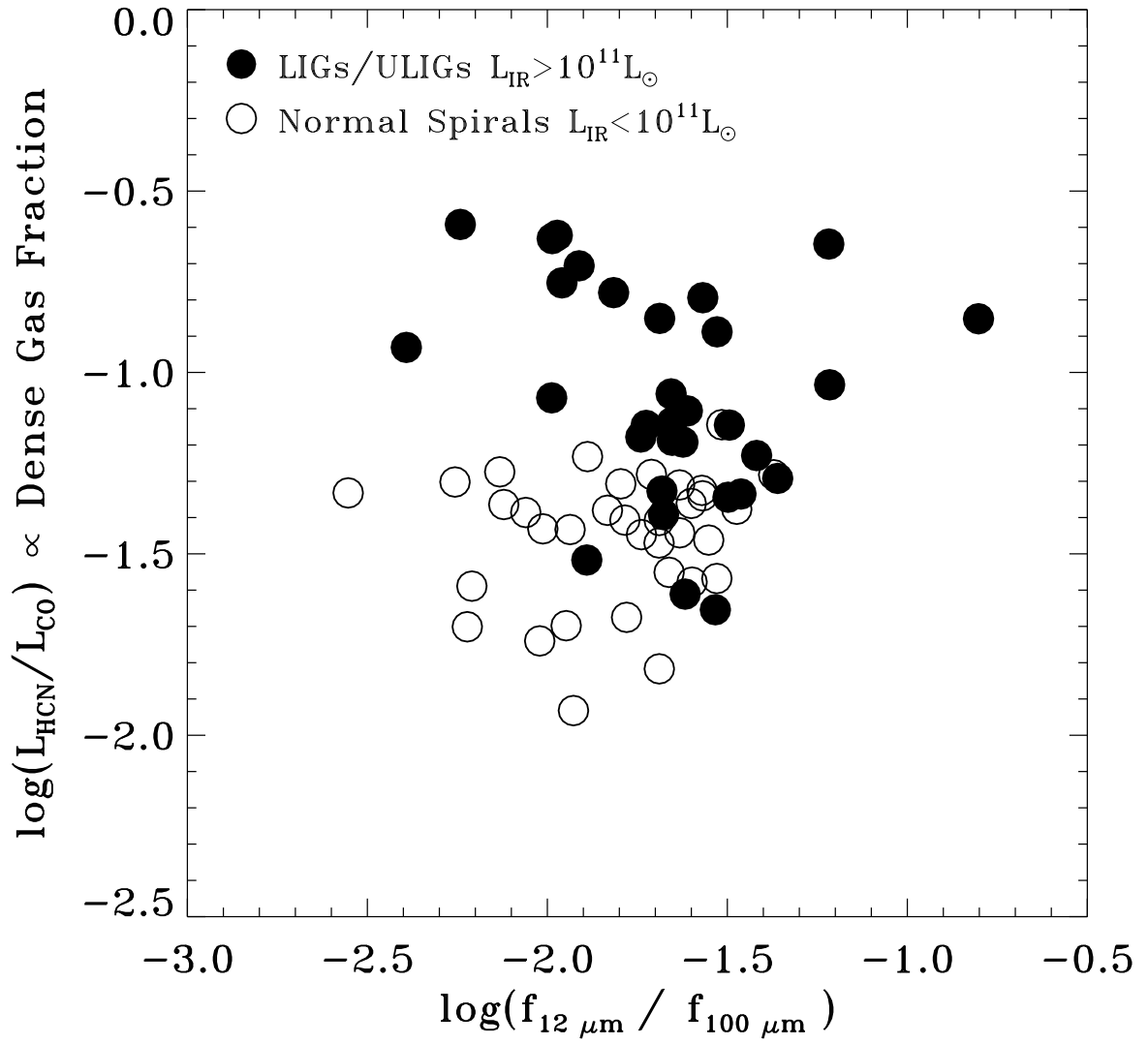


Fig. 5b

This figure "fg2a.gif" is available in "gif" format from:

<http://arxiv.org/ps/astro-ph/0310341v2>

This figure "fg2b.gif" is available in "gif" format from:

<http://arxiv.org/ps/astro-ph/0310341v2>

This figure "fg2c.gif" is available in "gif" format from:

<http://arxiv.org/ps/astro-ph/0310341v2>

This figure "fg3a.gif" is available in "gif" format from:

<http://arxiv.org/ps/astro-ph/0310341v2>

This figure "fg3b.gif" is available in "gif" format from:

<http://arxiv.org/ps/astro-ph/0310341v2>